國立臺灣大學工學院機械工程學研究所

碩士論文

Department of Mechanical Engineering

College of Engineering

National Taiwan University

Master Thesis

AOI 機台之結構最佳化與熱補償設計

Structural Optimum Design and Thermal

Compensation Design of an AOI Machine Structure

馬嘉宏

Chia-Hung Ma

指導教授：鍾添東 博士

Advisor: Tien-Tung Chung, Ph.D.

中華民國 99 年 7 月

July, 2010

國立臺灣大學碩士學位論文
口試委員會審定書

AOI 機台之結構最佳化與熱補償設計

Structural Optimum Design and Thermal Compensation Design of an AOI Machine Structure

本論文係馬嘉宏君（R95522638）在國立臺灣大學機械工程學系完成之碩士學位論文，於民國 99 年 07 月 27 日承下列考試委員審查通過及口試及格，特此證明

口試委員：（指導教授）

鍾添東 _____（簽名）

范光照 _____

劉正良 _____

系 主 任 _____（簽名）

Acknowledgments

感謝指導教授鍾添東老師三年來的辛勤指導與教誨，使本論文得以順利完成。也感謝口試委員范光照老師與劉正良老師對本論文的細心指正，使得本論文更臻完善。

回首研究所生涯並不如大部份人順遂。在經歷更換指導教授的事件，幸虧當時的錦德學長在我還沒進入此研究室，便已開始給我鼓勵。進入研究室後也並非事事順心，多虧研究夥伴小家、子揚、稍微、Jaran、嘟嘟、僅僅、Coolken、烏龜等人，大家互相提攜與照顧，才能順利一路走到今天。同時也感謝前後幾屆學長姐、學弟妹的陪伴，不管是後門、三國或是飛龍都有我們共同的回憶。要謝的人太多了，只好老梗的謝個天了。

最後要感謝我的父母、家人與女友元真，從不曾因為延畢的事情指責我並安慰我，讓我的心裡總是充滿溫暖。謹以此論文獻給每個關心我的人。

Structural Optimum Design and Thermal Compensation Design of an AOI Machine Structure

Abstract

This paper studies the optimum design and thermal compensation design of a high precision automatic optical inspection (AOI) machine structure. First, the structure of AOI machine is introduced. A parametric program for AOI machine is developed to generate solid models of the AOI machine automatically. Then, structural characteristics of the AOI machine are analyzed by the finite element analysis (FEA) and obtained by experiments. Structural responses, such as deformation of the base frame and inspection lens tip, of the original structure are analyzed. An integrated program is also developed by combining solid model generation, FEA simulation, response approximation and numerical optimization searches. Using this integrated program, optimum design of the machine base and moving parts of AOI machine are conducted. The results of optimum design improve the structural characteristics of the AOI machine structure. After the temperature distribution experiment, the thermal deformation of the AOI machine can be analyzed by FEA. Finally, a thermal compensation design is proposed to compensate this thermal error.

Keywords: Automatic optical inspection, structural optimum design, finite element analysis, thermal compensation design

AOI 機台之結構最佳化與熱補償設計

摘要

本文主要探討高精度自動化光學檢測(automatic optical inspection, AOI)機台結構的最佳化設計與熱補償設計。首先，介紹一種現有的 AOI 機台結構，並發展一套參數化實體模型繪圖程式以自動化更新此機台結構模型之主要設計參數。接著透過有限元素分析(finite element analysis, FEA)與實驗，得到此機台之結構特性。現有機台結構之各種結構響應(structural response)，諸如機台底座與檢測模組之變形量等，便可經由分析取得。一整合型最佳化程式亦被提出。此程式包括了四個部份：實體模型產生、有限元素分析模擬、行為響應近似模型產生與最佳化數值搜尋等。利用此整合型最佳化程式，對此 AOI 機台之底座結構與移動件分別進行最佳化設計。此最佳化之結果，將可改善底座結構與移動件之結構特性，如結構剛性增強與輕量化等。另經由溫度分佈實驗得到機台於工作達到穩態時之溫度分佈，便可利用有限元素分析得到機台之熱變形情形。最後提出一熱補償設計，來改善此熱膨脹變形情形。

關鍵詞：自動化光學檢測、結構最佳化設計、有限元素分析、熱補償設計

Table of Contents

List of Figures

XIII

List of Tables

List of Symbols

G	rate of heat generation
$\dot{g}$	rate of heat generation per unit volume
V	volume of heat generation medium
h	coefficient of convection heat transfer
k	coefficient of thermal conductivity
L_{vp}	characteristic length of the geometry
Nu	Nusselt number
Ra	Rayleigh number
Pr	Prandtl number
Gr	Grashof number
g	gravitational acceleration
β	coefficient of volume expansion
T_f	film temperature
T_s	temperature of surface
T_∞	temperature of the fluid sufficiently far from the surface
ν	kinematic viscosity of the fluid
L_{hp}	characteristic length of horizontal plate
A_{hp}	surface area of horizontal plate
P_{hp}	perimeter of horizontal plate
L_{hsp}	characteristic length of horizontal square plate

a_{hsp}	length of horizontal square plate
L_{hcp}	characteristic length of horizontal circular plate
D_{hcp}	diameter of horizontal circular plate
C	constant
m	constant
ρ	density of fluid
V	mean fluid velocity
d	diameter of tube
μ	dynamic viscosity
ε_T	thermal strain
ΔT	temperature change
α	coefficient of thermal expansion
σ	stress
P_{axial}	axial force
A_{bar}	cross section area of the bar
ε	strain
δ_{bar}	length change of bar
L_{bar}	bar length
E	modulus of elasticity
$\sigma_x,\ \sigma_y,\ \sigma_z$	stress in x, y, z directions
$\varepsilon_x,\ \varepsilon_y,\ \varepsilon_z$	strain in x, y, z directions
ν	Poisson's ratio

$\vec{x}$	design vector
$F(\vec{x})$	objective function
$g_i(\vec{x})$	i_{th} constraint
n_c	number of constraints
$U_x(\vec{x})$	maximum deformation in X direction
$U_y(\vec{x})$	maximum deformation in Y direction
$V_b(\vec{x})$	volume of base frame
$U_L(\vec{x})$	deformation at the inspection lens tip
$V_{XB}(\vec{x})$	volume of the X-axis beam
ΔT_{Xb}	average temperature variation of X-axis beam
ΔT_{LMs}	average temperature variation of linear motor stator
L_0	origin length of X-axis beam and linear motor stator
L_{Xb}	X-axis beam lengths by thermal expansion
L_{LMs}	linear motor stator lengths by thermal expansion
α_{Xb}	thermal expansion coefficient of X-axis beam
α_{LMs}	thermal expansion coefficient of linear motor stator
θ	bevel angle of thermal compensation design
α_A	thermal expansion coefficient of box and plate with I-shaped cross sections
α_B	thermal expansion coefficient of plate with rectangle-shaped

H_0 origin height of box and plates

H_A height of box and plate with I-shaped cross sections by thermal

               expansion

H_B height of plate with rectangle-shaped by thermal expansion

ΔT_{box} temperature change of box

n number of plates in a box

Chapter 1 Introduction

Due to the low profit rate, traditional industries have lost their competitiveness in the past two decades. The emerging technologies and hi-tech industries took advantage in meanwhile, and traditional industries are replaced by them as the key role of promoting the Taiwan economy growth, such as the IC, PC/NB, LCD, communication, MEMS and so on. In the hi-tech industries field, both the main on-line fabrication equipment as well as the off-line inspection equipment is indispensable to guarantee product quality. The on-line AOI equipment is to add AOI machines into production line, such that the AOI machine can full check all production in process. Configuration of on-line AOI equipment in production line [1] is shown as Fig. 1-1. The AOI equipment is the necessary tool in detecting the dimensions and the defects of the hi-tech components, in accordance with the trend of high throughput and high resolution.

The AOI equipment is imported in most domestic hi-tech industries. It consists of the integration of mechanical-electrical-optical-information technologies for technology need. Through the integration of its strong background in mechatronic technology in positioning stages with the optical image processing techniques, it is possible to promote a new AOI industry in Taiwan. The main reason to promote the AOI research for the coming years in Taiwan is because the market requirements are huge not only in domestic need but also in global need. IC, PCB, LCD, Communication, and MEMS parts are the focused industrial applications [2].
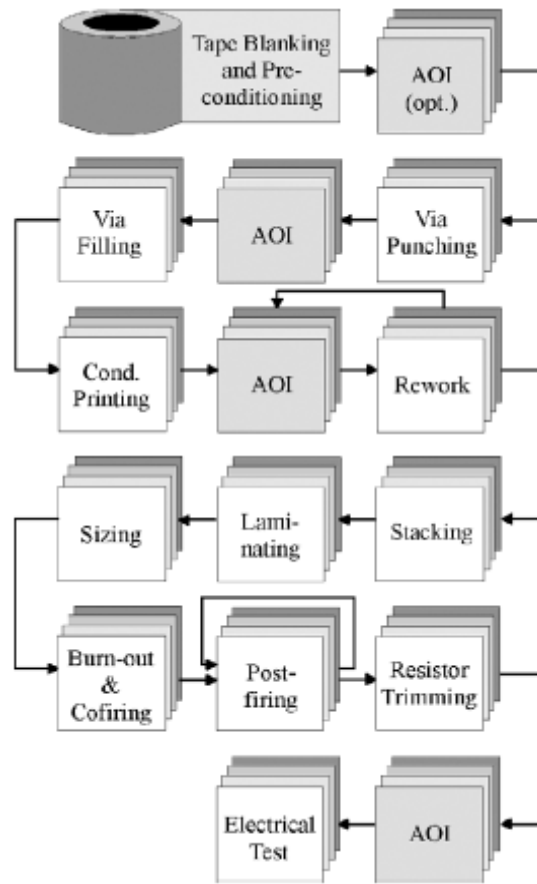
Figure 1-1 Configuration of on-line AOI machine in production line [1]

This paper studies regarding two topics about AOI machine. One is about the structure of AOI machine (gantry and base,) and another is about thermal compensation design.

To improve the structure of gantry and base, J.J. Wu develop a finite element model for a 1/10 scale crane rig in the laboratory, as Fig. 1-2 shown, so that one may predict the dynamic behavior of the scale crane rig based on the relevant features of the developed finite element model. The finite element model is then modified, according to the experimental results, using various techniques. It has been found that the new modified finite element model, by replacing the conventional infinite rigidity for the ground-fixed nodes by the appropriate stiffness for the translational and rotational springs, as Fig. 1-3 shown, can predict the vibration characteristics of the experimental

2

crane rig with satisfactory accuracy [3].
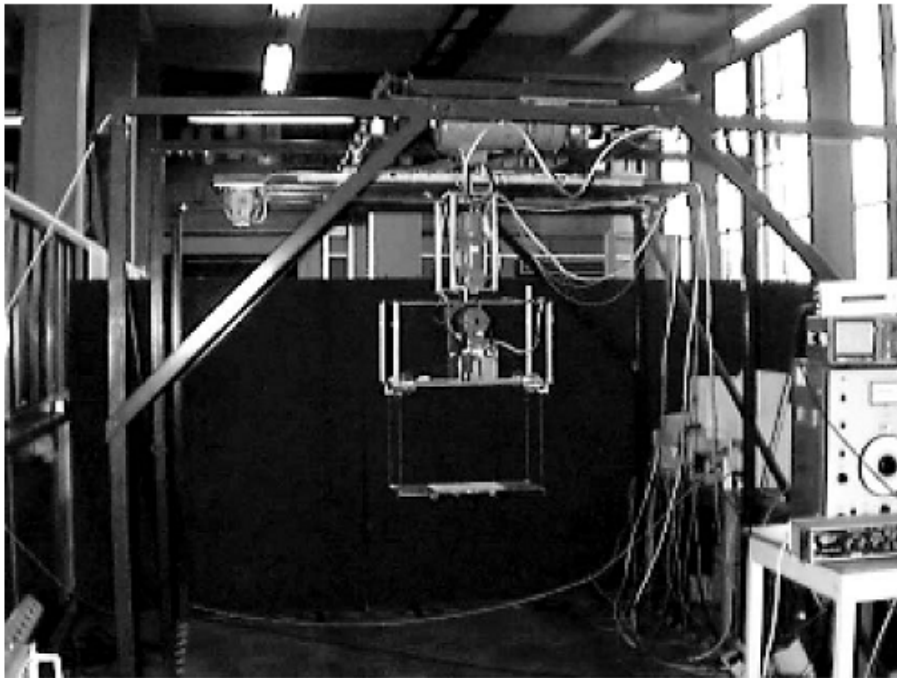
Figure 1-2 1/10 scale crane rig in laboratory [3]
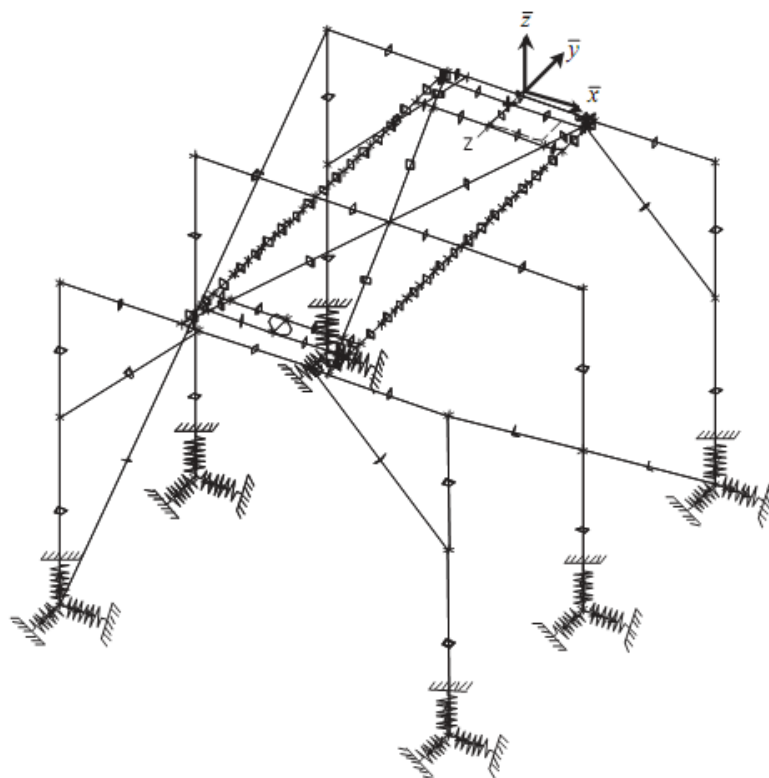
Figure 1-3 Modified finite element model of crane [3]

Jochen M. Rieber proposed a series automatic control methods for a compliant two-axes mechanism, as shown in Fig. 1-4. The investigation demonstrates how high-precision manufacturing tasks can be optimized by the integration of robot link design and control system design. A trade-off between mass reduction and motion time reduction is shown via a simulation study related to an industry-grade prototype gantry robot [4].
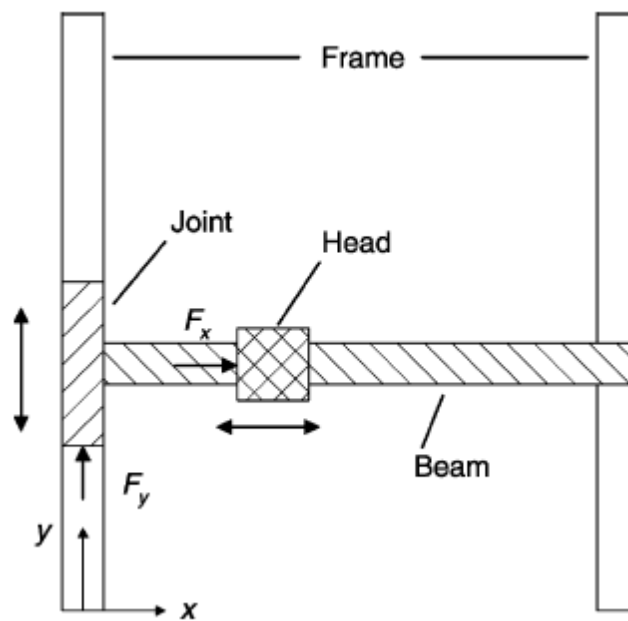
Figure 1-4 Simplified gantry robot configuration [4]

D.R. Griffiths proposed a method combined genetic algorithm and shape optimization to determine the optimal cross-section of beams, subject to various loading conditions. The initial test case is the evolution of an optimal I-beam cross-section, subject to several load cases, as shown in Fig. 1-5. It is shown that the methods developed lead to consistently good solutions, despite the complexity of the process [5].
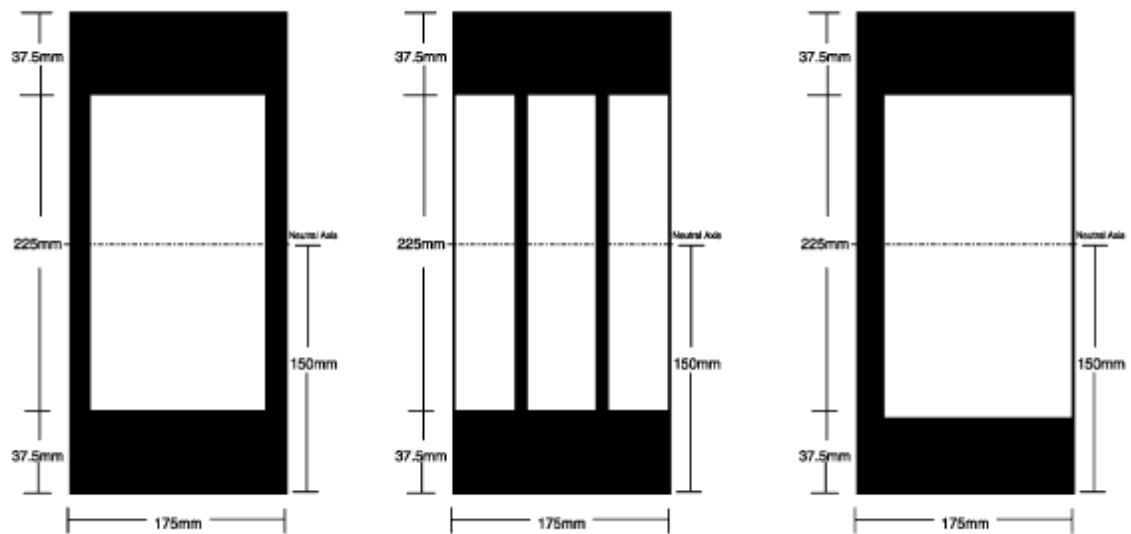
Figure 1-5 Alternative cross-sectional shapes for various loading [5]

Mathivanan studies on the dynamic behavior of a machine base for crankshaft pin milling machine. Design modifications are proposed to optimize the number of the ribs used and its thickness based on the static and dynamic analysis of the assembly, as shown in Fig. 1-6. A comparison between the existing and modified base structure which is reinforced with the concrete, is also discussed [6].
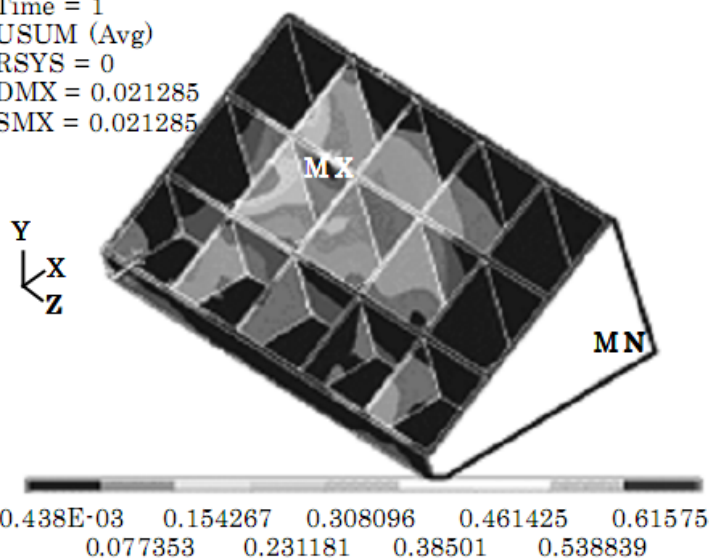
Figure 1-6 Stress distribution on the vertical ribs in the modified structure [6]

5

J. Gomand proposed that Industrial control of Dual-Drive Moving Gantry Stage Robots is usually achieved by two independent position controllers, as shown in Fig. 1-7. A physical dynamic lumped parameters model of an industrial robot based on structural, modal, and Finite Element Method analysis is proposed, experimentally identified and validated [7].
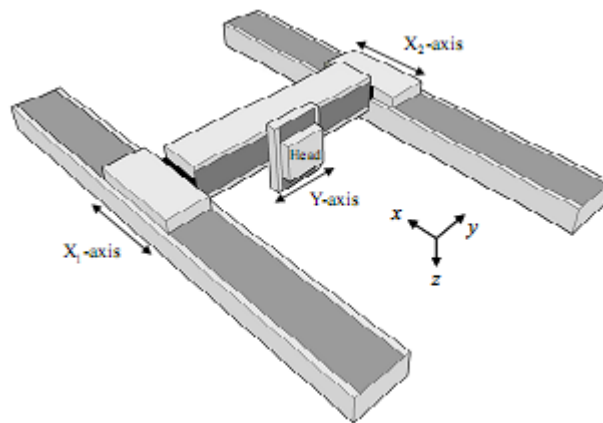
Figure 1-7 Symbolic representation of a dual-drive gantry system [7]

Based on the configuration principles of biological skeletons and sandwich stems, Ling Zhao proposed a machine tool column with stiffening ribs inside was designed using structural bionic method, as shown in Fig. 1-8. After the lightening effect was verified by finite element simulation, scale-down models of a conventional column and a bionic column were fabricated and tested. Results indicate that the bionic column can reduce the maximum static displacement by 45.9% with 6.13% mass reduction and its dynamic performances is also better with increases in the first two natural frequencies [8].
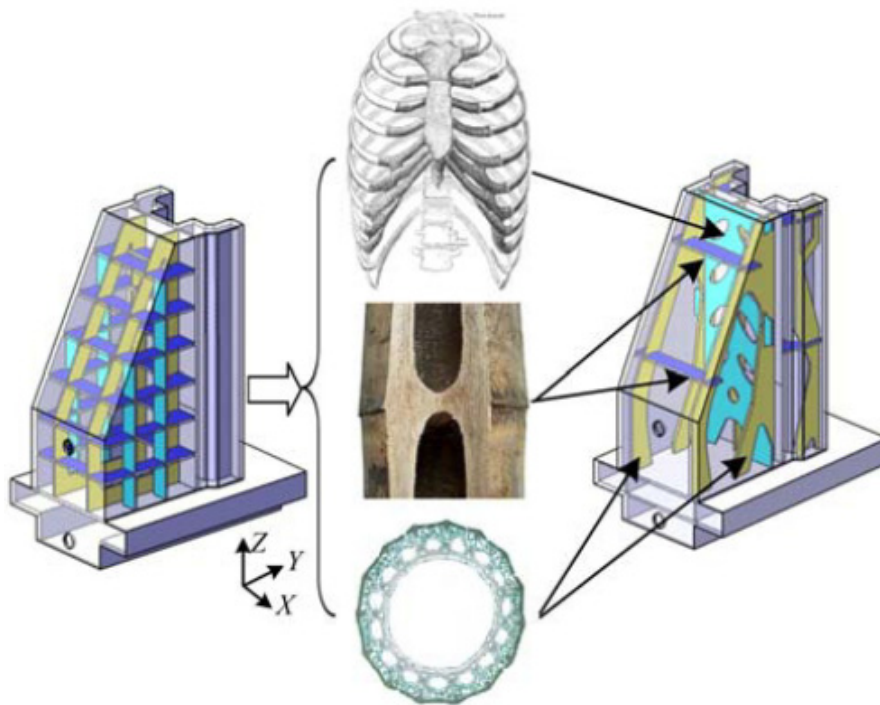
Figure 1-8 Structural bionic design of stiffening ribs [8]

S. C. Jung design an imperfection detecting machine which has composite–aluminum hybrid beam structure with high-modulus carbon/epoxy composites in order to enhance dynamic stiffness and damping capacity of the structure. New designs of beam structure are also proposed for the next generation inspecting system which has much longer beam length, as shown in Fig. 1-9. Parametric study for composite X-axis beam system and optimization scheme of joint inserts are performed in the designing process [9].
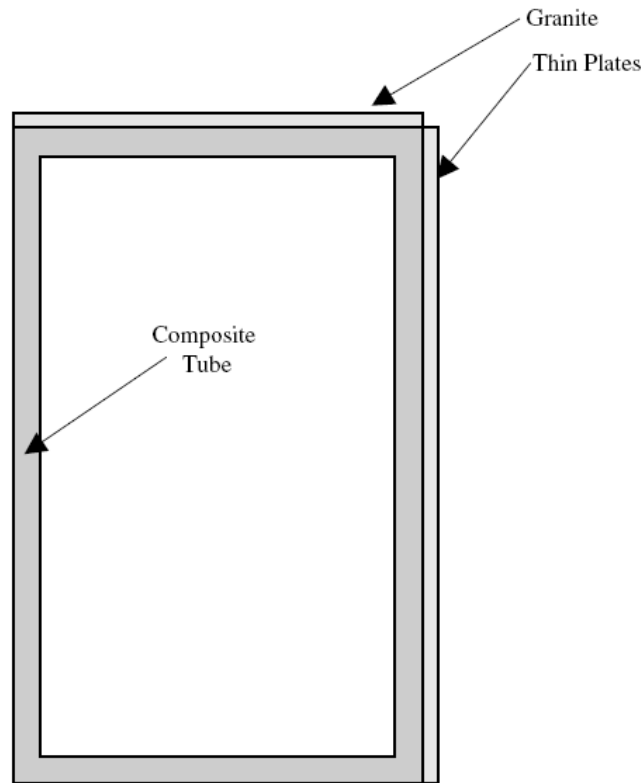
Figure 1-9 Composite X-axis beam for the next generation LCD detecting machine [9]

In order to enhance structural robustness of microfactory machine elements, Ju Ho Kim proposed the foam-composite sandwich structure. Unidirectional carbon/epoxy prepreg as skin materials and PVC foams as core materials were used to construct the sandwich structures, as shown in Fig. 1-10. and 1-11. The total mass of the sandwich column system was 1 kg whereas the mass of the current aluminum system was 2.6 kg. From the vibration tests it was found that the newly designed sandwich column system had 1.5 times higher natural frequency [10].
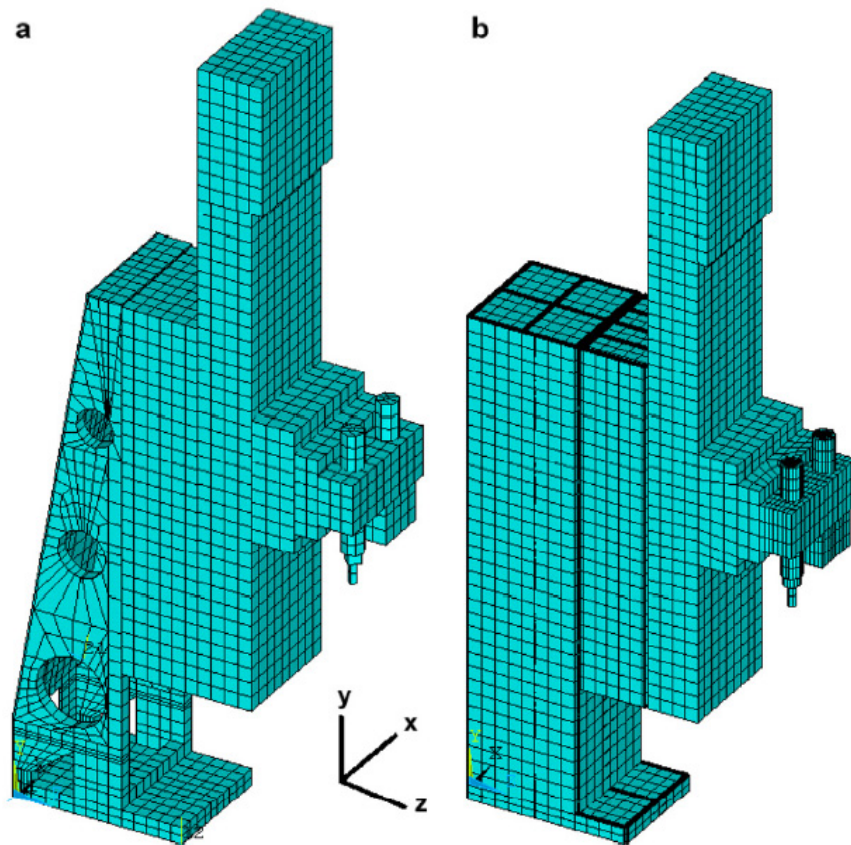
Figure 1-10 Finite element models of (a) the aluminum system and (b) the foam-composite
sandwich system [10]
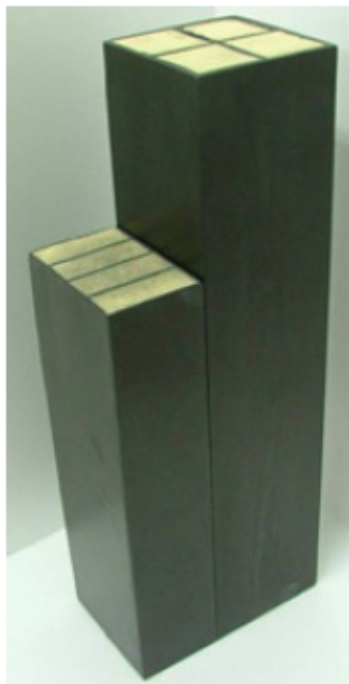
Figure 1-11 The foam-composite sandwich structures [10]

To consider about thermal effect on machines, Sun-Kyu Lee proposed the effects on machine slide-guide contact conditions caused by thermal deformation, as shown in Fig. 1-12. Since a slide guide as a large friction surface, the motion is greatly influenced by thermal distortion caused by heat generation in the ball nut and the bearing support, during machining processes. This can investigate the typical behavior of the friction coefficient in response to both the external load and the linear speed [11].
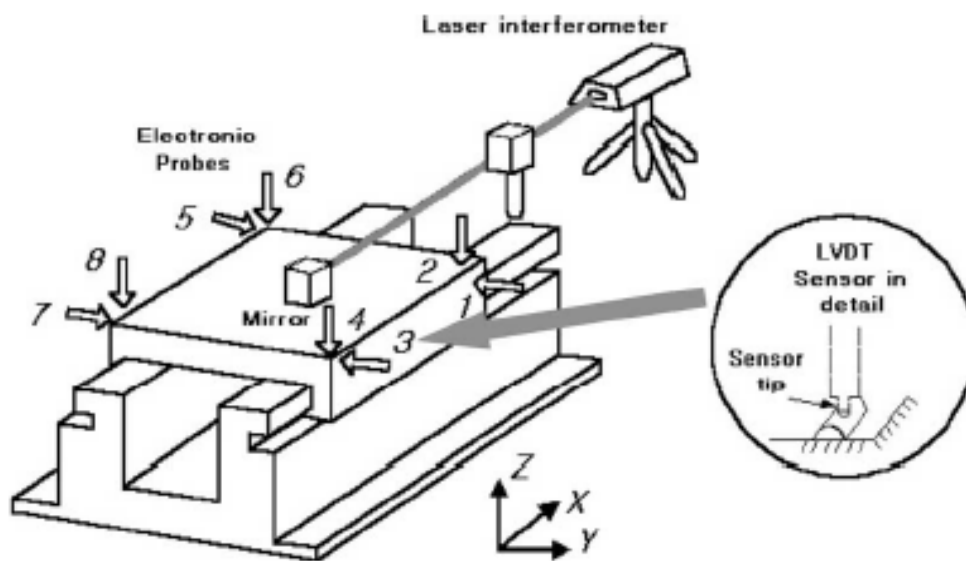
Figure 1-12 Measurement of thermal effect on slide-guide [11]

E. Creighton proposed a spindle growth compensation scheme that aims towards reducing its thermally-induced machining errors. A FEA is conducted on the spindle assembly. This FEA correlates the temperature rise, due to heating from the spindle bearings and the motor, to the resulting structural deformation. It is expected to reduce its thermally induced spindle displacement by 80% [12], as shown in Fig. 1-13.
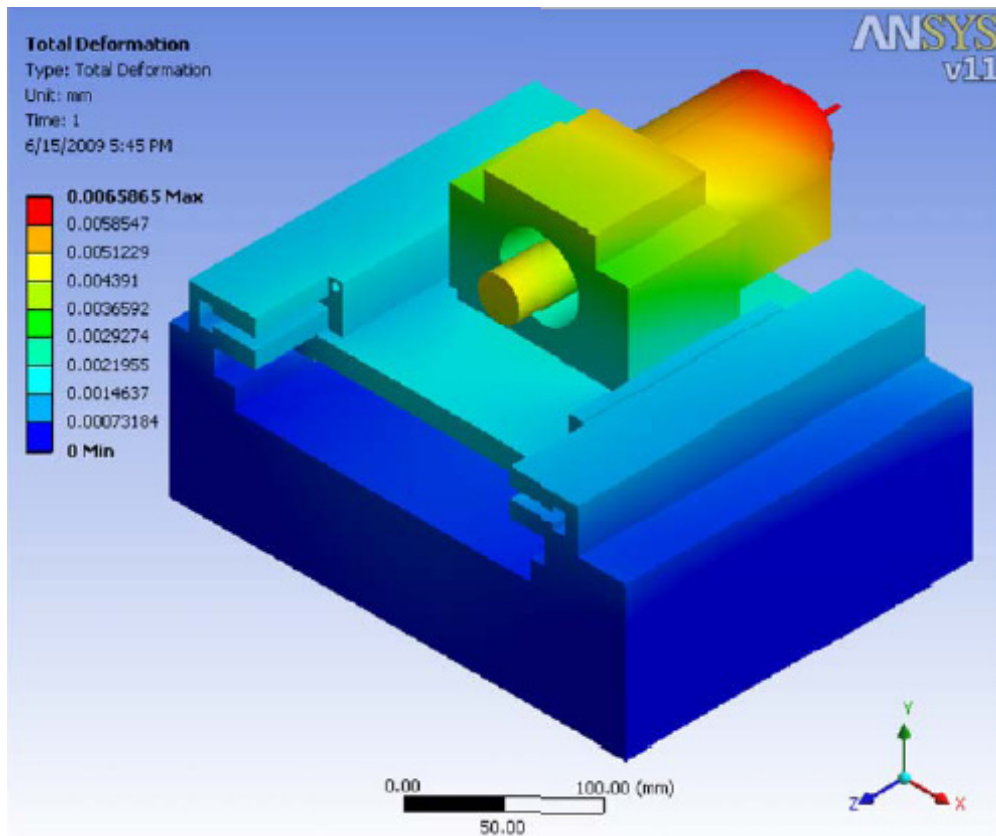
Figure 1-13 Spindle, motor and housing under thermal stresses [12]

A. Gelman proposed passive thermal compensation mechanism is intended for maintaining the stability of performance parameters of an optomechatronic system over a wide operating temperature range, as shown in Fig. 1-14. This allows the mechanism described herein to act as a motion amplifier. The amplifier Input is a small dimensional change in the links, caused by temperature change and its output is the rotational motion of the output link. The amplification is according to the rules of lever dynamics [13].

11
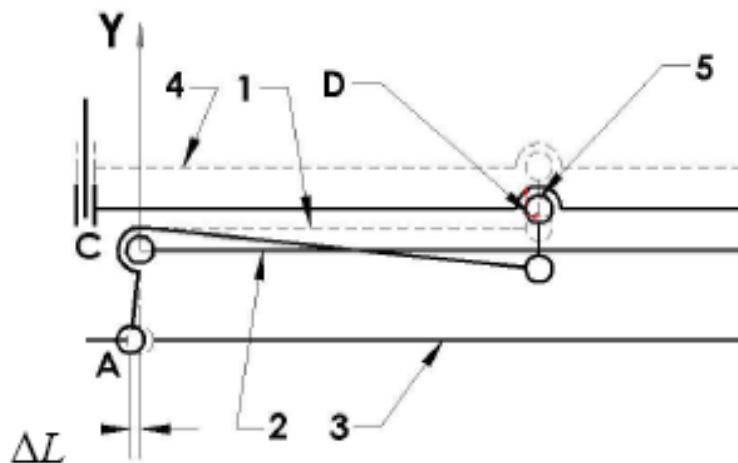
Figure 1-14 Operating sequence of the mechanism when temperature changes [13]

Mark Stern proposed a load cell temperature compensation system for accurately measuring a force load applied to an external member during environmentally varying temperature values. It includes a standard load cell which is rigidly mounted on a load cell mounting plate, as shown in Fig. 1-15. The load cell mounting plate is fixedly secured to the external member which has an external force load applied thereto. The temperature compensation system further includes a force load application mechanism which transmits a predetermined force load to the load cell. In this manner, temperature variations applied to the external member will be compensated for by compensation system and not read as a load force applied to the external member [14].
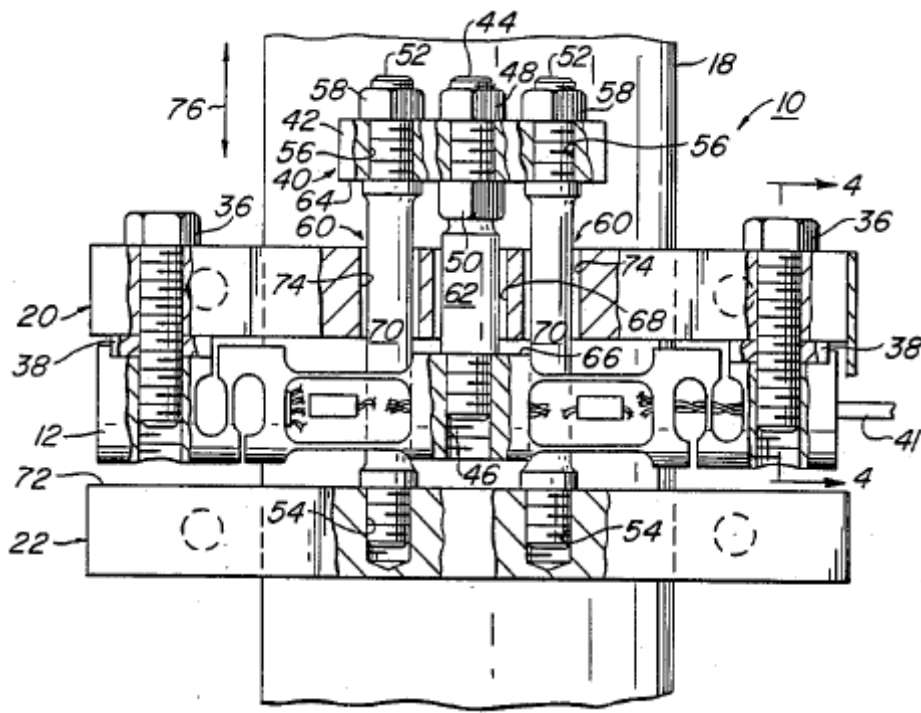
Figure 1-15 Elevation view of load cell temperature compensation system [14]

Michael J. proposed an athermalized optical assembly includes a laser beam source, such as a laser diode, and a collimator lens which are together mounted in an active thermally-compensated structure, as shown in Fig. 1-16. The difference in the coefficient of thermal expansion (CTE) of each compensation ring is chosen such that the flexure plate kinematic hinge is passively operated to approximately compensate for thermal shifts in system focal length while maintaining radial and angular alignment of the lens relative to the laser diode source, so as to provide controlled axial movement of the collimating lens [15].

13
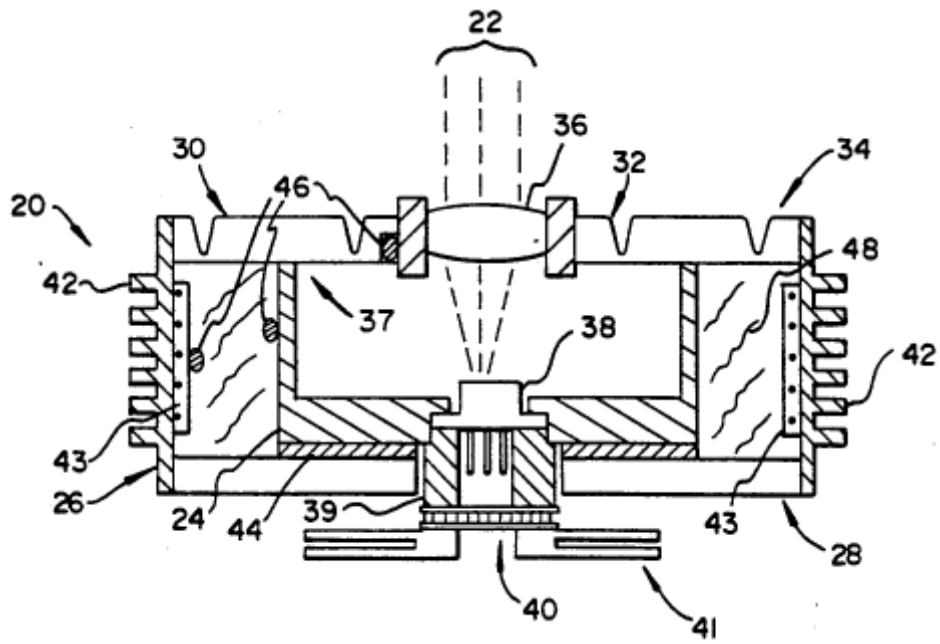
Figure 1-16 A section view of an optical assembly [15]

Donald R. proposed a passive mechanical system that unwanted positional shifts between two objects, such as lenses, are precisely compensated during thermal changes, as shown in Fig. 1-17. Materials with differing coefficients of thermal expansion and angled interfaces transforms a longitudinal dimensional change into a fine transverse dimensional change to precisely control movement as a function of temperature thereby maintaining, e.g., lens focus [16].
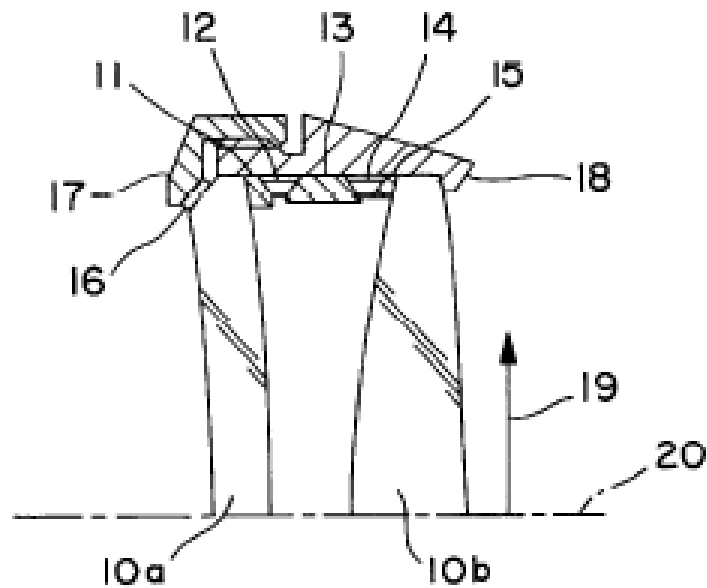
Figure 1-17 Invention involving four interfaces used in a lens mount [16]

This paper aims at providing a structural optimum design and a local thermal compensation design for AOI machine. First, the structure of AOI machine is introduced. Secondly, the static analysis of AOI machine is performed by considering the effect of inertial force. Thirdly, various types of base design are proposed to improve the structural strength of AOI machine. Based on the analysis, the structural optimum design is performed to provide a suitable design for AOI machine base. Fourthly, the optimum designs of moving part are also performed to both reduce weight and deformation separately. Fifthly, the temperature distribution analysis is proposed by considering operating conditions, and the thermal deformation analysis is also performed. Finally, there is a new thermal designs proposed for reducing the thermal deformation generated by the difference in the coefficient of thermal expansion of X-axis beam and linear motor stator.

Chapter 2 Theory and Development of AOI Machine Structure

2.1 Evaluation of Heat Generation and Air Convection Coefficients

This paper refers to the book of HEAT TRANSFER [17] for the thermal analysis. A medium through which heat is conducted may involve the conversion of electrical, nuclear, or chemical energy into heat energy. In heat conduction analysis, such conversion processes are characterized as heat generation. The rate of heat generation in medium may vary with time as well as position within the medium. When the variation of heat generation with position is known, the total rate of heat generation in a medium of volume V can be determined from:

$$G = \int_V \dot{g} d\mathrm{V} \tag{2-1}$$

In the special case of uniform heat generation, as in the case of electric resistance heating throughout a homogeneous material, the relation in Eq. 2-1 reduces to $G = \dot{g}\mathrm{V}$, where $\dot{g}$ is the constant rate of heat generation per unit volume.

Natural convection heat transfer on a surface depends on the geometry of the surface as well as its orientation. It also depends on the variation of temperature on the surface and the thermo-physical properties of the fluid involved. The simple empirical formulations for calculating the coefficient of convection heat transfer h in natural convection are divided into two parts, vertical plate part and horizontal plate part. For vertical plates, the formulations can be expressed as Eq. 2-2 to Eq. 2-4.

$$h = \frac{k}{L_{vp}} Nu \tag{2-2}$$

$$Nu^{1/2} = 0.825 + \frac{0.387 Ra^{1/6}}{\left[1 + \left(0.492 / Pr \right)^{9/16} \right]^{8/27}} \tag{2-3}$$

$$Ra = Gr \times Pr = \frac{g\beta(T_s - T_\infty)L_{vp}^{3}}{v^2} \times Pr \tag{2-4}$$

where k is coefficient of thermal conductivity, L_{vp} is characteristic length of the geometry, Nu is Nusselt number, Ra is Rayleigh number, Pr is Prandtl number, Gr is Grashof number, g is gravitational acceleration, β is coefficient of volume expansion, T_s is temperature of surface, T_∞ is temperature of the fluid sufficiently far from the surface, and v is kinematic viscosity of the fluid. Noting that all fluid properties are to be evaluated at the film temperature $T_f = \frac{1}{2}(T_s + T_\infty)$.

However, the characteristic length L_{hp} of horizontal plates is different than vertical plates and it can be calculated from:

$$L_{hp} = \frac{A_{hp}}{P_{hp}} \tag{2-5}$$

where A_{hp} is the surface area and P_{hp} is the perimeter. Note that $L_{hsp} = a_{hsp}/4$ for a horizontal square surface of length a_{hsp}, and $L_{hcp} = D_{hcp}/4$ for a horizontal circular surface of diameter D_{hcp}.

The rate of heat transfer to or from a horizontal surface depends on whether the surface is facing upward or downward. After calculating the characteristic length L_{hp}

of horizontal plates by Eq. 2-5, the simple empirical formulations for calculating the coefficient of convection heat transfer h in natural convection are similar to the formulations of vertical plates and it can be expressed as Eq. 2-6 to Eq. 2-8.

$$h = \frac{k}{L_{hp}} Nu \tag{2-6}$$

$$Nu = C \times Ra^m \tag{2-7}$$

$$Ra = \mathrm{Gr}\,\mathrm{Pr} = \frac{g\beta(T_s - T_\infty)L_{hp}{}^3}{v^2} \times \mathrm{Pr} \tag{2-8}$$

where the values of the constants C and m depend on the geometry of the surface and the flow region, which is characterized by the range of the Rayleigh number. The constant C is 0.54 and the value of m is 1/4 in this paper.

Flow in a tube can be laminar or turbulent, depending on the flow conditions. Fluid flow is streamlined and thus laminar at low velocities, but turns turbulent as the velocity is increased beyond a critical value. It certainly desirable to have precise values of Rayleigh numbers for laminar, transitional, and turbulent flows. Under most practical conditions, the flow in a tube is laminar for $Ra < 2300$, turbulent for $Ra > 10000$, and transitional in between. The Reynolds number is defined as Eq. 2-9.

$$Ra = \frac{\rho V d}{\mu} \tag{2-9}$$

where ρ is the density, V is the mean fluid velocity, d is the diameter of the tube, and μ is the dynamic viscosity.

The average Nusselt number for turbulent flow across tubes can be expressed compactly as Eq. 2-10 and Eq. 2-11.

$$Nu = CRa^m \Pr^n \tag{2-10}$$

$$h = \frac{k}{d} Nu \tag{2-11}$$

where Rayleigh numbers Ra can be defined by Eq. 2-9. Noting that $C = 0.023$, $m = 0.8$, and $n = 0.3$ are given in this paper for cooling condition.

2.2 Thermal Deformation Analysis of AOI Machine Structure

Changes in temperature produce expansion or contraction of structural materials, resulting in thermal strains and thermal stresses. A simple illustration of thermal expansion is shown in Fig. 2-1, where the block of material is unrestrained and therefore free to expand [18]. When the block is heated, every element of the material undergoes thermal strains in all directions, and consequently the dimensions of the block increase.

Linear expansion
$$\frac{\Delta L}{L_0} = \alpha \Delta T$$

Area expansion
$$\frac{\Delta A}{A_0} = 2\alpha \Delta T$$

Volume expansion
$$\frac{\Delta V}{V_0} = 3\alpha \Delta T$$
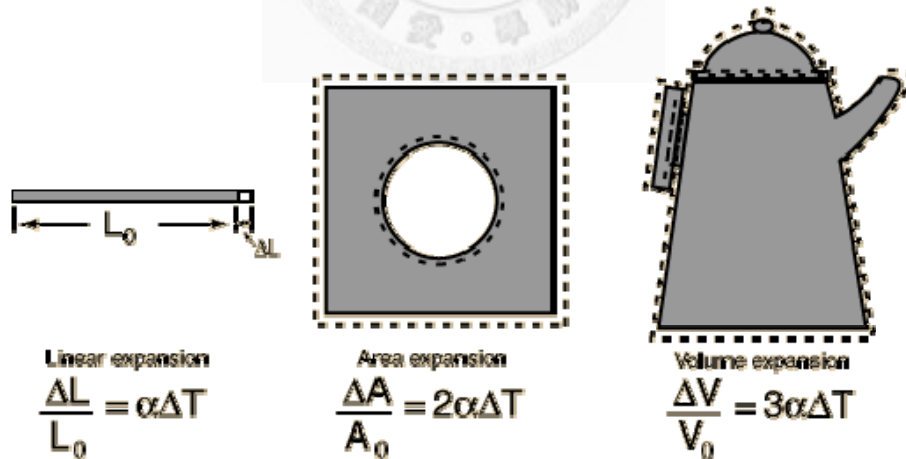
Figure 2-1 A simple illustration of thermal expansion [18]

This paper refers to the book of Mechanics of Materials for thermal deformation analysis [18]. For most structural materials, thermal strain ε_T is proportional to the temperature change $\varDelta T$; that is,

$$\varepsilon_T = \alpha(\Delta T) \tag{2-12}$$

in which α is a property of the material called the coefficient of thermal expansion. Since strain is a dimensionless quantity, the coefficient of thermal expansion has units equal to the reciprocal of temperature change. In SI units the dimensions of α can be expressed as either 1/K (the reciprocal of kelvins) or 1/°C (the reciprocal of degrees Celsius).

In general, the force per unit area is called the stress and is denoted by the Greek letter σ. Thus, the axial force P_{axial} acting at the cross section is the resultant of the continuously distributed stresses. Assuming that the stresses are uniformly distributed over cross section, the resultant must be equal to the intensity σ times the cross-section area A_{bar} of the bar. Therefore, the stresses can be expressed as:

$$\sigma = \frac{P_{axial}}{A_{bar}} \tag{2-13}$$

This equation gives the intensity of uniform stress in an axially loaded, prismatic bar of arbitrary cross section shape. When the bar is stretched by the forces P_{axial}, the stresses are tensile stresses; if the forces are reversed in direction, causing the bar to be compressed, the stresses are compressive stresses.

As already observed, a straight bar will change in length when loaded axially, becoming longer when in tension and shorter when in compression. Therefore, a unit length of the bar will have an elongation equal to $1/L_{bar}$ times δ_{bar}. This quantity is called the elongation per unit length, or strain, and is denoted by the Greek letter ε. The strain is given by the Eq. 2-14. If the bar is in tension, the strain is called a tensile strain, representing an elongation or stretching of the material. If the bar is in

compression, the strain is a compressive strain and the bar shortens.

$$\varepsilon = \frac{\delta_{bar}}{L_{bar}}$$ (2-14)

Many structural materials, including most metals, wood, plastics, and ceramics, behave both elastically and linearly when first loaded. Consequently, the stress-strain curves begin with a straight line passing through the origin. When a material behaves elastically and also exhibits a linear relationship between stress and strain, it is said to be linearly elastic.

The linear relationship between stress and strain for a bar in simple tension or compression is expressed by the Eq. 2-15 and is called Hooke's law. Noting that E is a constant of proportionality known as the modulus of elasticity for the material. The modulus of elasticity is the slope of the stress-strain diagram in the linearly elastic region.

$$\sigma = E\varepsilon$$ (2-15)

If the material follows Hooke's law, the strains produced by the stresses σ_x, σ_y, and σ_z acting independently are superimposed to obtain the resultant strains ε_x, ε_y, and ε_z. Thus, the following equations for the strains in tri-axial stress can be expressed as Eq. 2-16. Noting that v is Poisson's ratio and E is the modulus of elasticity.

$$\begin{cases} \varepsilon_x = \frac{1}{E}\left[\sigma_x - v\left(\sigma_y + \sigma_z\right)\right] \\ \varepsilon_y = \frac{1}{E}\left[\sigma_y - v\left(\sigma_z + \sigma_x\right)\right] \\ \varepsilon_z = \frac{1}{E}\left[\sigma_z - v\left(\sigma_x + \sigma_y\right)\right] \end{cases}$$ (2-16)

Therefore, combining Eq. 2-12 with Eq. 2-16 for the thermal strain in Hooke's law:

22

$$\begin{cases} \varepsilon_x = \dfrac{1}{E}\left[\sigma_x - v\left(\sigma_y + \sigma_z\right)\right] + \alpha \varDelta T \\[2mm] \varepsilon_y = \dfrac{1}{E}\left[\sigma_y - v\left(\sigma_z + \sigma_x\right)\right] + \alpha \varDelta T \\[2mm] \varepsilon_z = \dfrac{1}{E}\left[\sigma_z - v\left(\sigma_x + \sigma_y\right)\right] + \alpha \varDelta T \end{cases} \qquad (2\text{-}17)$$

Ordinary structural materials expand when heated and contract when cooled, and therefore an increase in temperature produce a positive thermal strain. Assuming that the material is homogeneous and isotropic and that the temperature increases $\varDelta T$ is uniform throughout the block. This equation can calculate the increase in any dimension of the block by multiplying the original dimension by the thermal strain. If one of the dimensions is L_{bar}, then that dimension will increase by the amount.

$$\delta_{bar} = \varepsilon_T \times L_{bar} = \alpha \times \varDelta T \times L_{bar} \qquad (2\text{-}18)$$

$$\sigma = E\varepsilon_T = E(\alpha \times \varDelta T) \qquad (2\text{-}19)$$

Chapter 3 Analysis of AOI Machine Structure

In order to determine the specification of the AOI machine, a finite element analysis was performed. The structure of AOI machine is introduced. Finite element model of AOI machine structure is also proposed. Due to the inertial force produced from moving parts during detection process, the analysis of AOI machine is conducted to understand the characteristics of AOI machine structure. The result of analysis is also verified by experiment result.

3.1 Structure of AOI Machine

An AOI machine is generally composed of a base, a X-axis beam, a Y-axis beam, and the inspection unit. The AOI machine to be analyzed in this paper has gantry type structure as shown in Fig. 3-1. The gantry structure is mounted on a base and the devices under test are placed on the base.
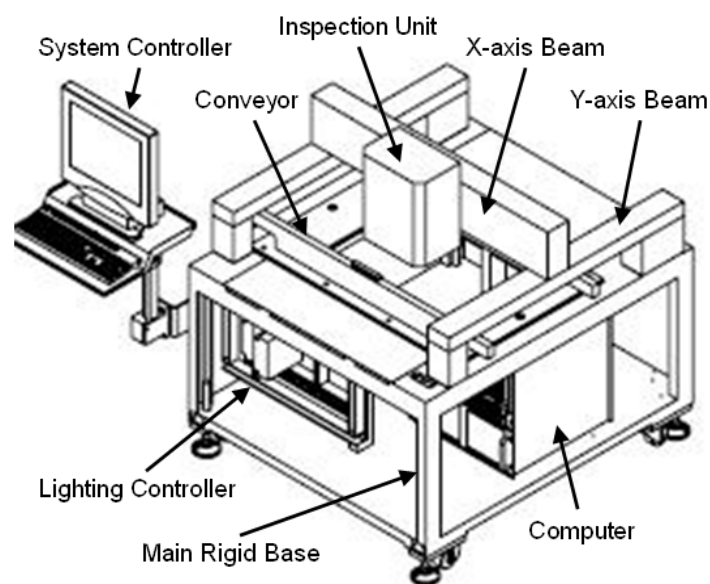
Figure 3-1 Structure of a general gantry type AOI machine

3.2 Parametric Design of AOI Machine Structure

Based on the parametric design and feature tree, SolidWorks utilizes a parametric feature based approach to create models and assemblies. In a solid model, there are a lot of parameters in every feature. But not all parameters are interested by designers. The graphic user interface (GUI) is proposed to show the interesting parameters. Designers can update the shown parameters of model by GUI dialog conveniently. In this section, two kinds of parametric design programs are developed by Microsoft Visual Basic language. One is for AOI machine structure with GUI and the other is for any cad model from SolidWorks by executables (EXE files).

The GUI parametric design program includes several parts: menu items, schematic diagram, eDrawing viewer, file control and design parameters, as shown as Fig. 3-2. This program can update not only the length, width and height of whole machine, but also the cross section detail dimensions of X-axis beam, Y-axis beam and base frame. There are a total of 31 parameters. Based on this GUI parametric design program, designer who has no 3D modeling capability can update the CAD model parameters easily. The origin machine and double width of machine are shown in Fig. 3-3.

The other way to update the model parameters is the executables. In this paper, two executables are developed. They are controlled by command line arguments. Designers can update parameter by command "SW_PChange <part_name.sldprt> <parameter_name> <value>" and export ACIS model by command "SW_OutputSAT <part_name.sldprt> <part_name.sat>". Through these two executables, other program can automatically update SolidWorks model parameters and export SolidWorks CAD model to SAT file. It can then be imported into FEA software.
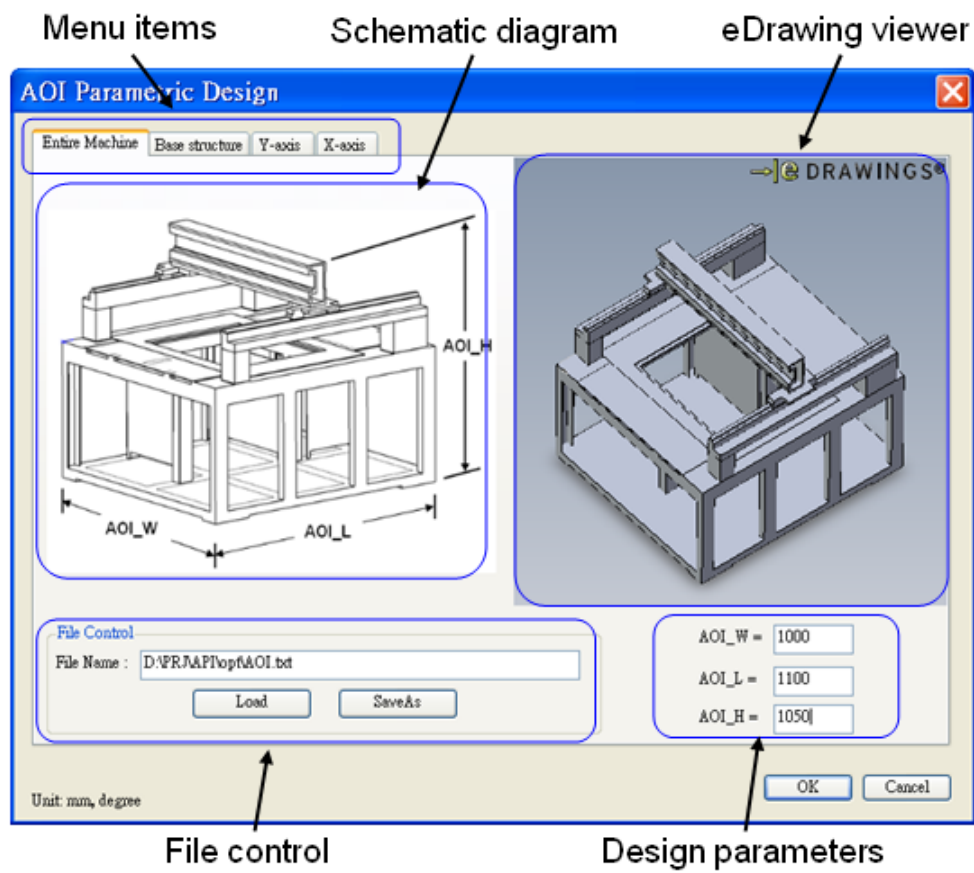
Figure 3-2 GUI parametric design program
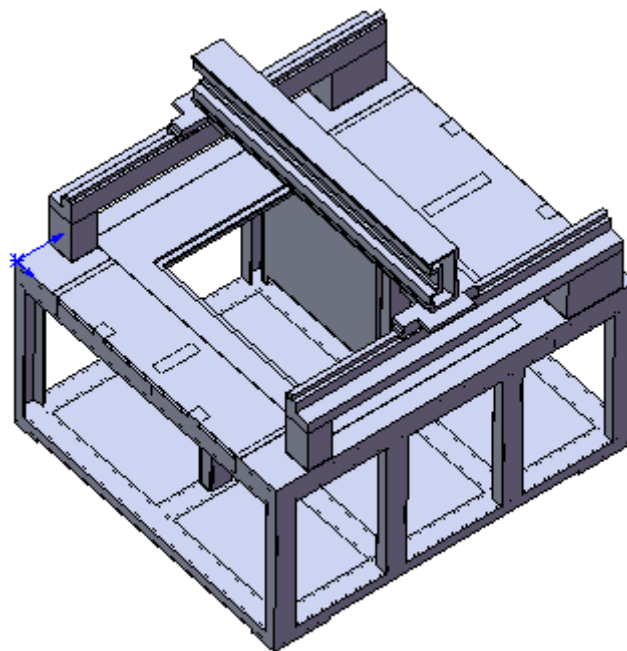
(a) Present AOI machine structure
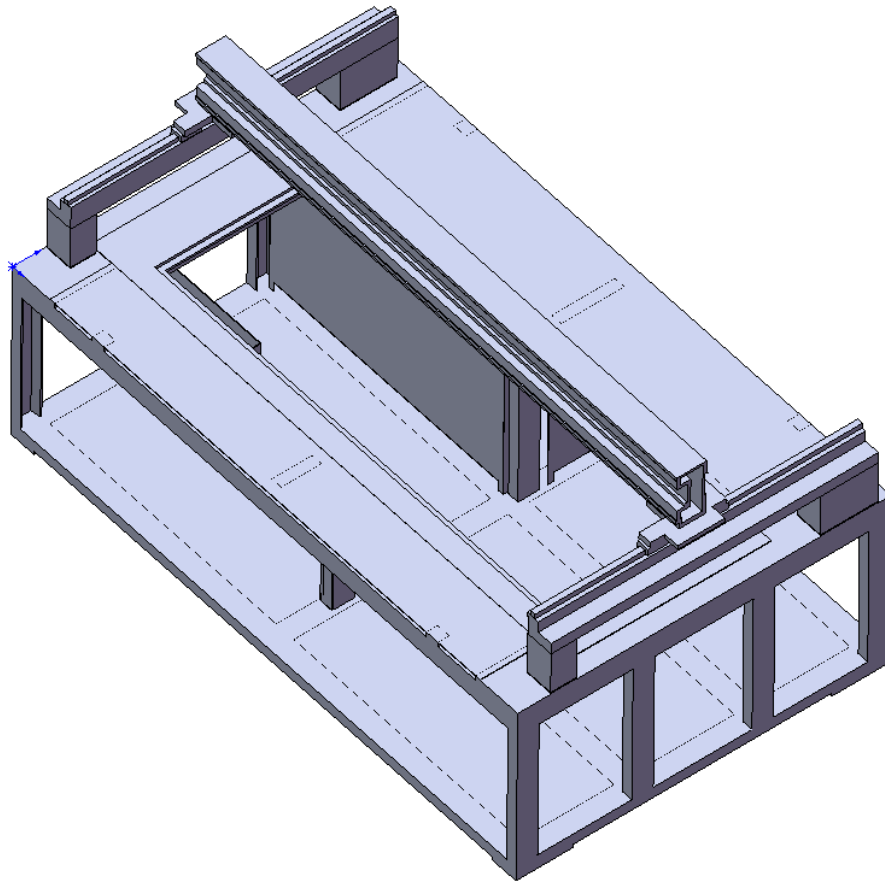
(b) AOI machine structure with double width

Figure 3-3 Parametric design of AOI machine structure

3.3 Finite Element Model of AOI Machine Structure

The solid model is transformed in the form of ACIS SAT, and then it is imported into finite element analysis software. Solid95, the structural second order element [19] as shown in Fig. 3-4, is used for modeling of AOI machine. Material properties are listed in Table 3-1.

About the boundary conditions, the displacements in Z-axis direction of four identical surfaces which contact with ground are set to zero. The displacements in X-axis and Y-axis directions are set to zero in one of four points, as shown in Fig. 3-5. In this way, AOI machine would not be over-constrained, and can deform in both

X-direction and Y-direction.
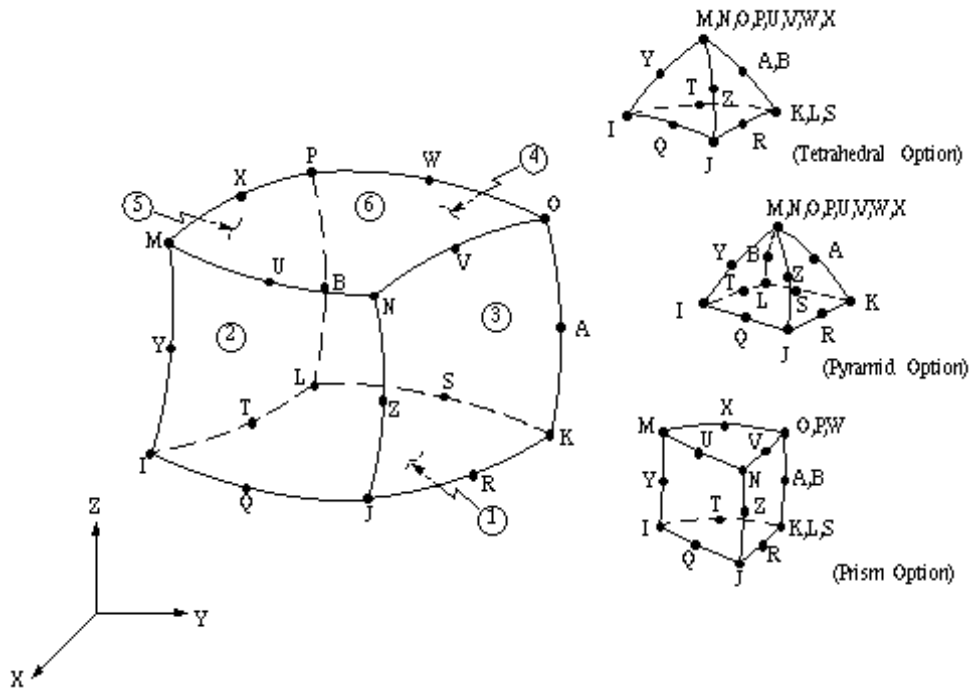
Figure 3-4 SOLID95 3D 20-node structural element in ANSYS [19]

Table 3-1 Material properties of AOI machine

Component	Material name	Young's modulus (GPa)	Poisson's ratio	Density (g/cm^3)
X-axis beam, stage and inspection unit	AL6061	68.9	0.33	2.7
Junction plate	AL7075	71.7	0.33	2.81
Linear guide	S50C	195	0.29	7.86
Y-axis beam	S45C	205	0.29	7.85
All other parts	SS41	205	0.29	7.85
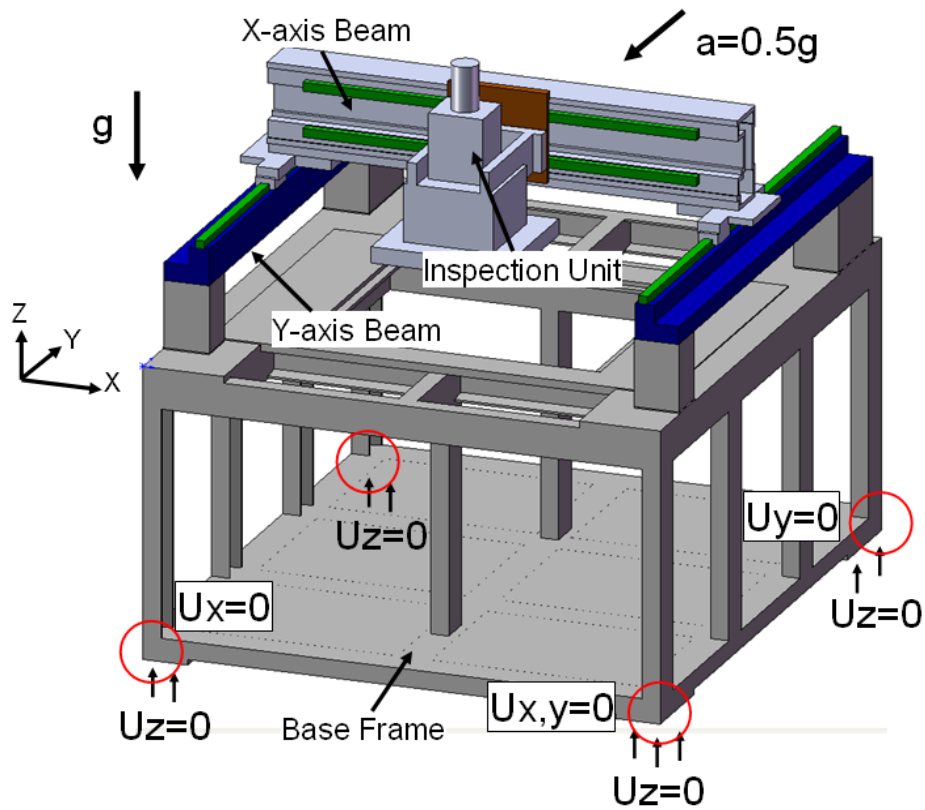
Figure 3-5 Boundary conditions of AOI machine

Tetra mesh was mainly used for mesh processing. Element number is between 55,000 and 60,000. After giving material properties and boundary conditions, a finite element mesh model is built, as shown in Fig. 3-6. One static FEM computation takes about 90 second at a computer equipped with Intel core 2 quad Q6600 CPU and 2 GB RAM.
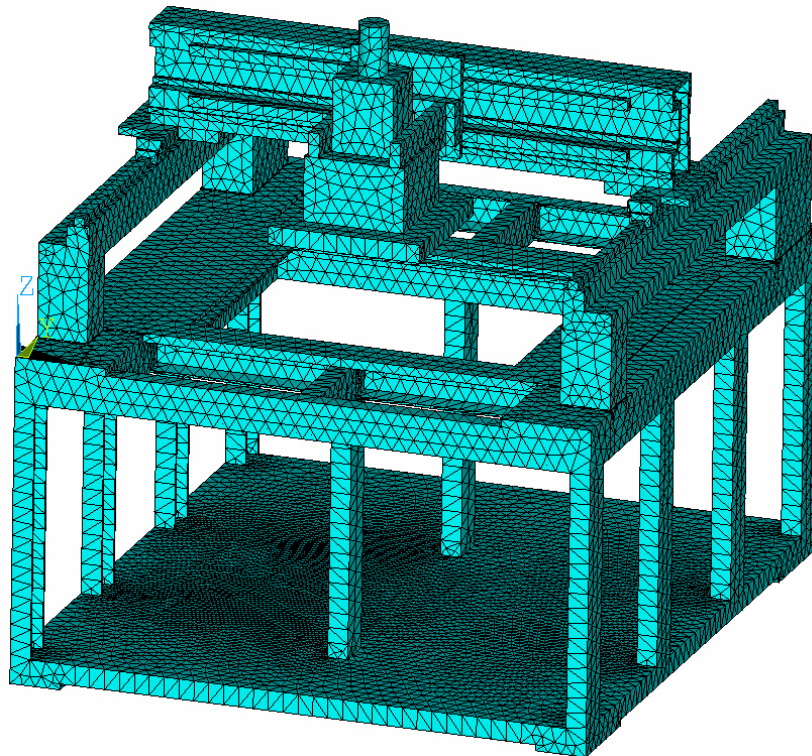
Figure 3-6 Mesh model of AOI machine

3.4 Structural Deformation Analysis and Experiments

Since the effect of gravity cannot be removed, the deflection due to self weight cannot be measured. To ensure the accuracy of the finite element model, an experiment is conducted by adding loads to AOI machine. The AOI machine is applied static 10kg per time at the upper middle point as the circle in figure, until the load reaches 50 kg, as shown in Fig. 3-7. The digimatic indicator of Mitutoyo, 543-563, is used to measure the deformation. It has 2.5μm accuracy and 0.5μm resolution, as shown in Fig. 3-8. This experiment had been conducted three times and digital indicator was used to measure deformation at specific points. The deformation versus load is linear.

Figure 3-7 Static deformation experiment set up

Metric			
Resolution	Order No.*	Range	Accuracy
0.0005mm, 0.001mm	543-561	30.4mm	0.0015mm
	543-563	60.9mm	0.0025mm

(a) A front view of 543-563   (b) Specifications of 543-563

Figure 3-8 Mitutoyo digimatic indicator 543-563

After comparing experiment results with FEM simulation results, if results are coherent, then the finite element modal is reliable. Since the result of deformation experiment 18.01μm corresponds with the result of FEM deformation 19μm as shown in Fig. 3-9, the FEM analysis error is 5.21%. Therefore, this finite element model can guarantee the accuracy of simulation.
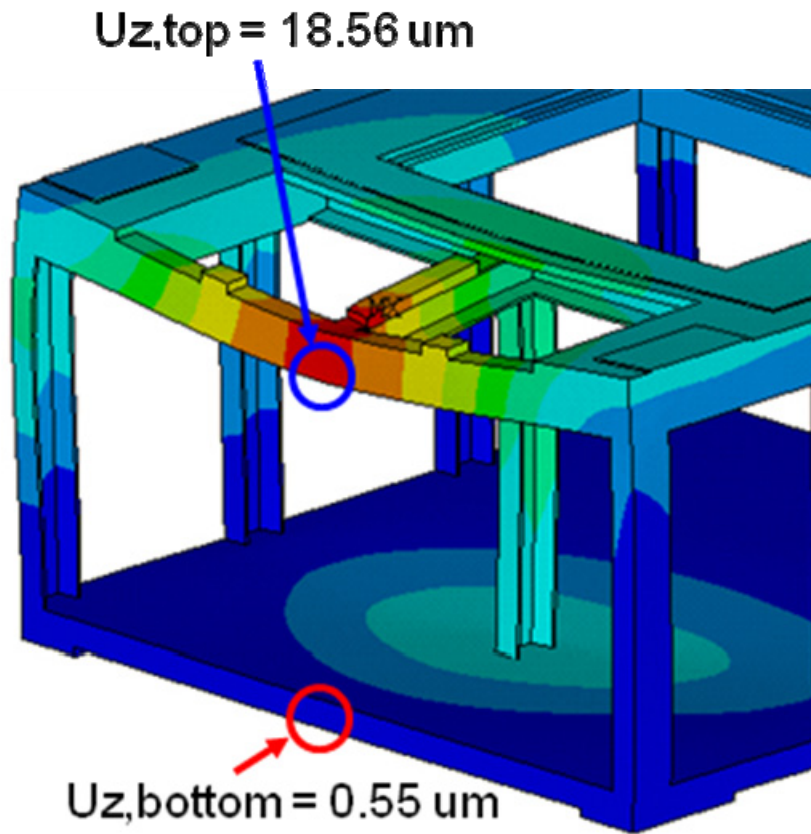
Figure 3-9 The simulation result

3.5 Deformation Due to Inertial Force

During the detection process, the inspection unit needs to move back and forward rapidly along X-axis, both the inspection unit and X-axis beam have to move back and forward rapidly along Y-axis, as Fig. 3-10 shown. The maximum acceleration of the inspection unit will reach 0.5g. Hence, when considering high precision, the effect of inertial force must be taken into consideration. There are two loading cases should be considered. Load case one is that the inspection unit moves along X-axis with the acceleration of 0.5g. Load case two is that the inspection unit and X-axis beam move along Y-axis with the acceleration of 0.5g, as Table 3-2 shown.

After taking the effect of inertial force into consideration, the simulation is conducted by using the FEM. The results of simulation are also listed in Table 3-2. The

displacement distribution of AOI machine is performed, too. In load case one, the maximum deformation of base is 12.45μm, and the maximum deformation of whole AOI machine is 34.02μm, as shown in Fig. 3-11. On the contrary, in load case two, the maximum deformation of base is 7.07μm, and the maximum deformation of whole AOI machine is 23.91μm.
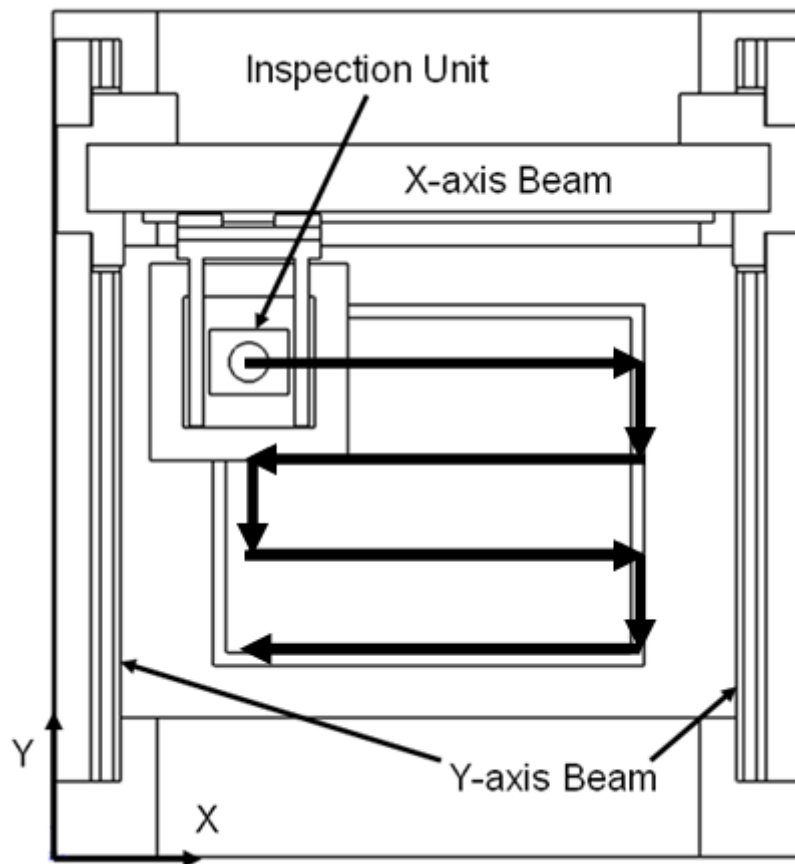
Figure 3-10 The inspection unit moves along X-axis and Y-axis

Table 3-2 Maximum deformation due to inertial force

Inertia loading	Acceleration	Max. deformation	Deformation of base
Load case 1, moving along X	(0.5g, 0, 0)	34.02μm	12.45μm
Load case 2, moving along Y	(0, 0.5g, 0)	23.91μm	7.07μm
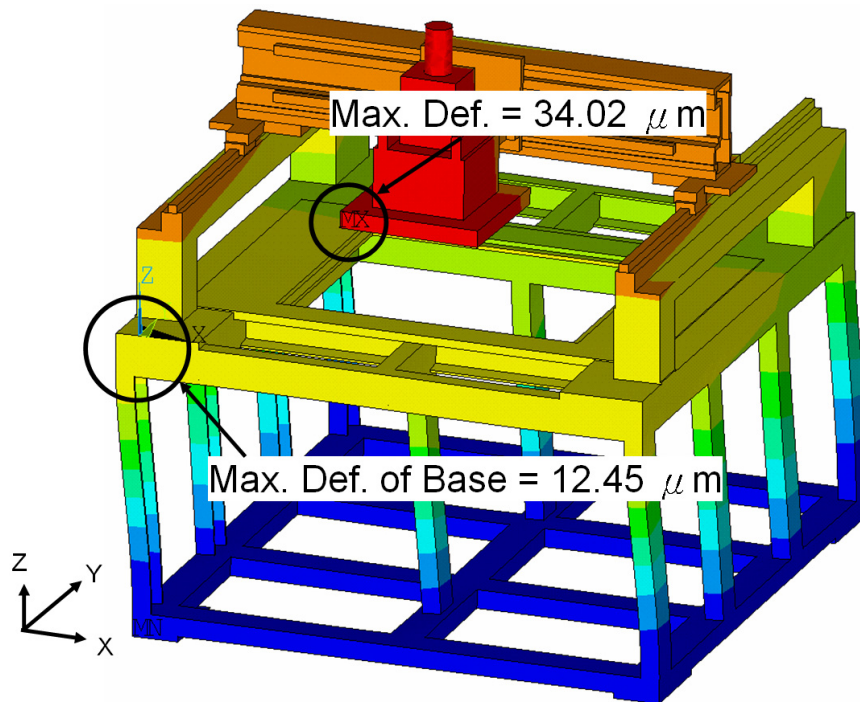
Figure 3-11 Displacement distribution due to inertial force (Load Case 1)

3.6 Modal Analysis and Modal Test

The purpose of modal test and modal analysis is to find out the natural frequencies and mode shapes of the structure. Not only the inspection unit of AOI machine moves back and forward during the detection process but also the others pumps, which fixed the objects by atmospheric pressure, and ball screws, which control the position of inspection unit, give the AOI machine structure steady oscillation forces back and forward. If the frequencies of this oscillation force are similar with any natural frequency of the structure, the structure may cause resonance. The detection accuracy will be affected. In this section, the modal test of AOI machine is proposed, and the modal analysis is also proposed to verify with each other.

For the accuracy of modal analysis, multipoint constraint element MPC184 is used, since there is one DOF between the X-axis beam and Y-axis beams by sliders. In ANSYS, MPC184 is multipoint constraint element which implements kinematic

35

constraints like rigid link, rigid beam, slider, spherical, revolute, universal and slot. In this case, the MPC184 slider constraint is used, its geometry is as shown as Fig. 3-12. The node I is expected to lie initially on the line joining the node J and K.
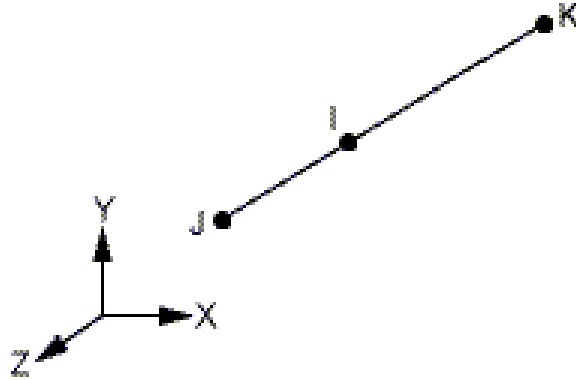
Figure 3-12 MPC184 slider constraint geometry [19]

Since there is no related displacement between machine base and ground, the four corners of the base bottom are fixed. Furthermore, X-axis beam is fixed with Y-axis beams by two angle plates for regular constraints, as shown as Fig. 3-13. Other boundaries and constraints are as the same as said in section 3-3. The results of the modal analysis about the X-axis beam of AOI machine are obtained by FEA. Less than 1000 Hz, natural frequencies of the AOI machine X-axis beam are 141Hz, 349Hz, 391Hz, 635Hz, 685Hz and 794Hz. The mode shapes of AOI machine at 141Hz, 349Hz, 635Hz and 794Hz are shown in Fig. 3-14.
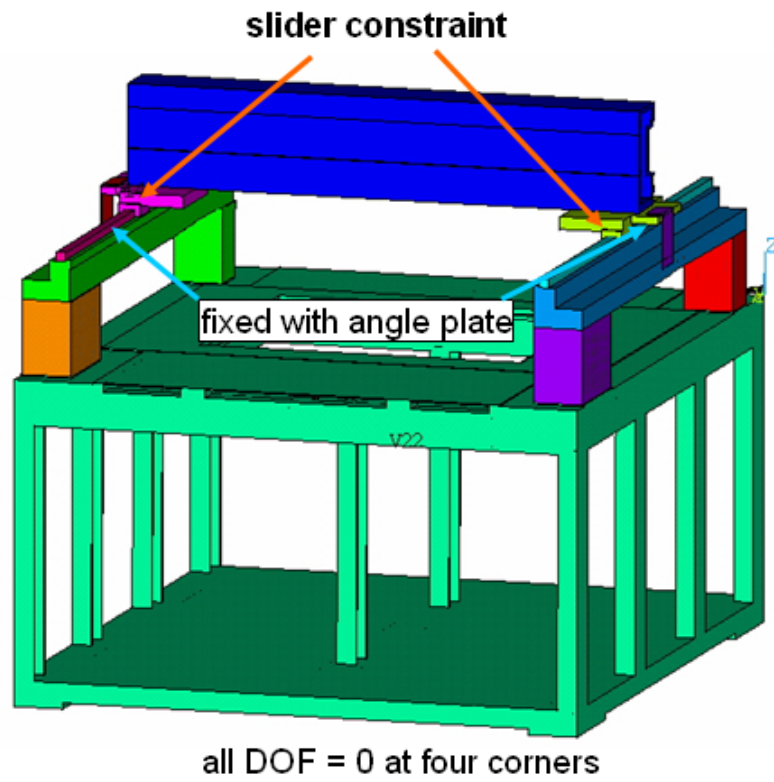
Figure 3-13 Boundaries of the AOI machine modal analysis
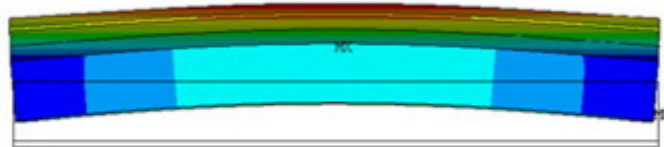
(a) Mode shape of X-axis beam at 141Hz
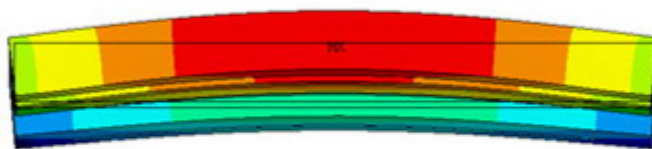
(b) Mode shape of X-axis beam at 349Hz

(c) Mode shape of X-axis beam at 635Hz
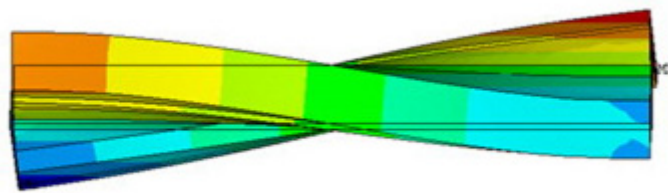
(d) Mode shape of X-axis beam at 794Hz

Figure 3-14 Mode shapes of AOI machine by FEM

The LDV (laser doppler vibrometer) is used to measure the natural frequencies and mode shapes of the AOI structure. LDV is a velocity measuring instrument, as shown in Fig. 3-15. The measurement principle of LDV is as follows: first, LDV injects a He-Ne laser, then the laser separates to reference beam and measurement beam by the spectroscope; second, the measurement beam reflects from vibrating object, therefore its wave length is initially 633 nm and variation after reflection; third, the detector detects sum of the reference beam and reflected measurement beam to compute the vibration frequencies of vibrating object; as shown as Fig. 3-16.

Figure 3-15 The laser doppler vibrometer [20]
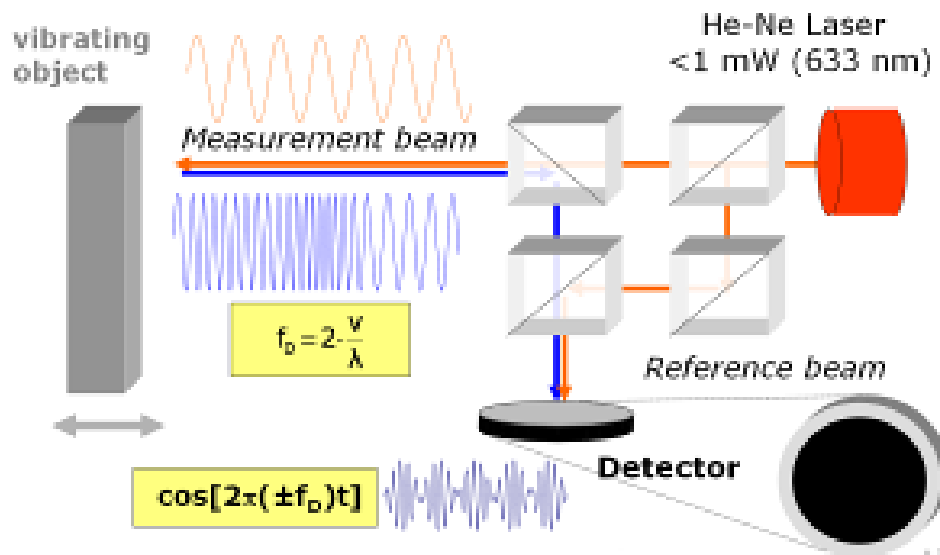
Figure 3-16 The laser doppler vibrometer principle schematic [20]

The boundary conditions are set as previously described. The results of the modal test about the X-axis beam of AOI machine are measured by LDV. Less than 1000 Hz, natural frequencies of the AOI machine X-axis beam are 131Hz, 324Hz, 375Hz, 582Hz, 645Hz and 724Hz. The mode shapes of AOI machine at 131Hz, 324Hz, 582Hz and 724Hz are shown in Fig. 3-17. Compared with the results of modal test and modal analysis, the maximum error is about 9.7%. It means that this FEM model is suitable to analyze with suitable boundaries.
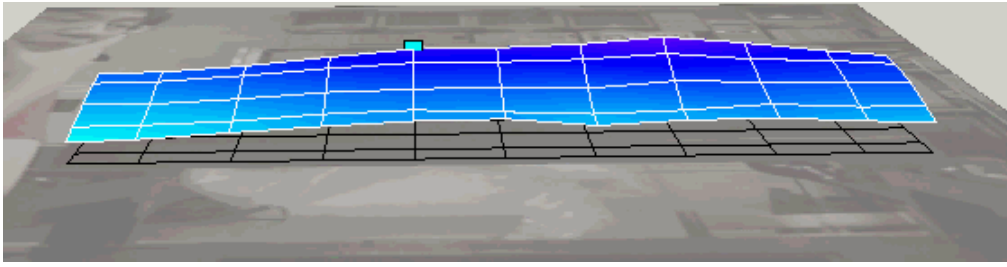
(a) Mode shape of X-axis beam at 131Hz
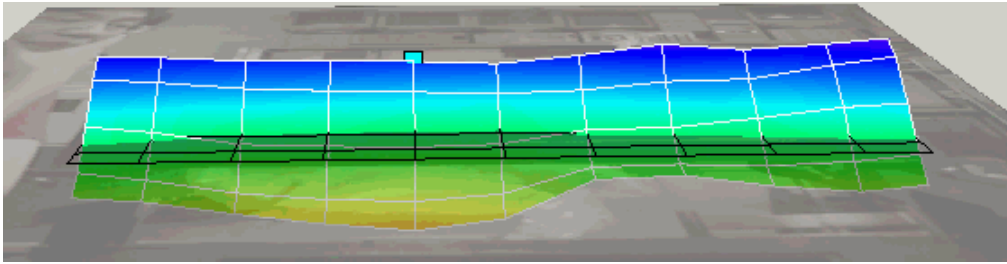
(b) Mode shape of X-axis beam at 324Hz
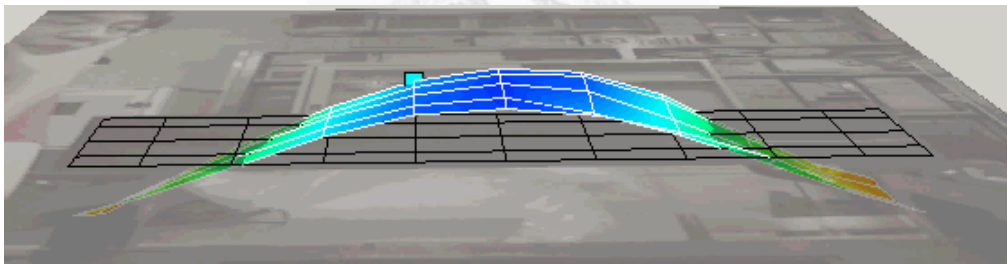
(c) Mode shape of X-axis beam at 582Hz
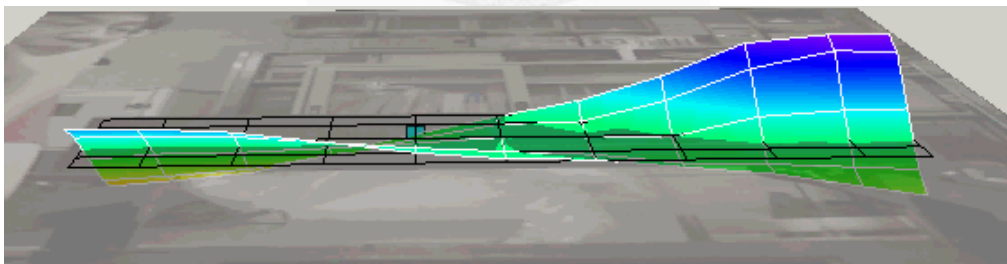
(d) Mode shape of X-axis beam at 724Hz

Figure 3-17 Mode shapes of AOI machine by LDV

3.7 Concept of Structural Optimum Design Program

The optimum design program is developed with four modules: model generation, FEA simulation, approximation and optimization, as shown in Fig. 3-18. This program

is written in Microsoft Visual C++ language. By parametric design program (SolidWorks API) and parametric analysis (ANSYS APDL), this program can update parameters of models, analyze automatically, and then execute sensitivity analysis and optimization. After several iterations, an optimal solution can be received.
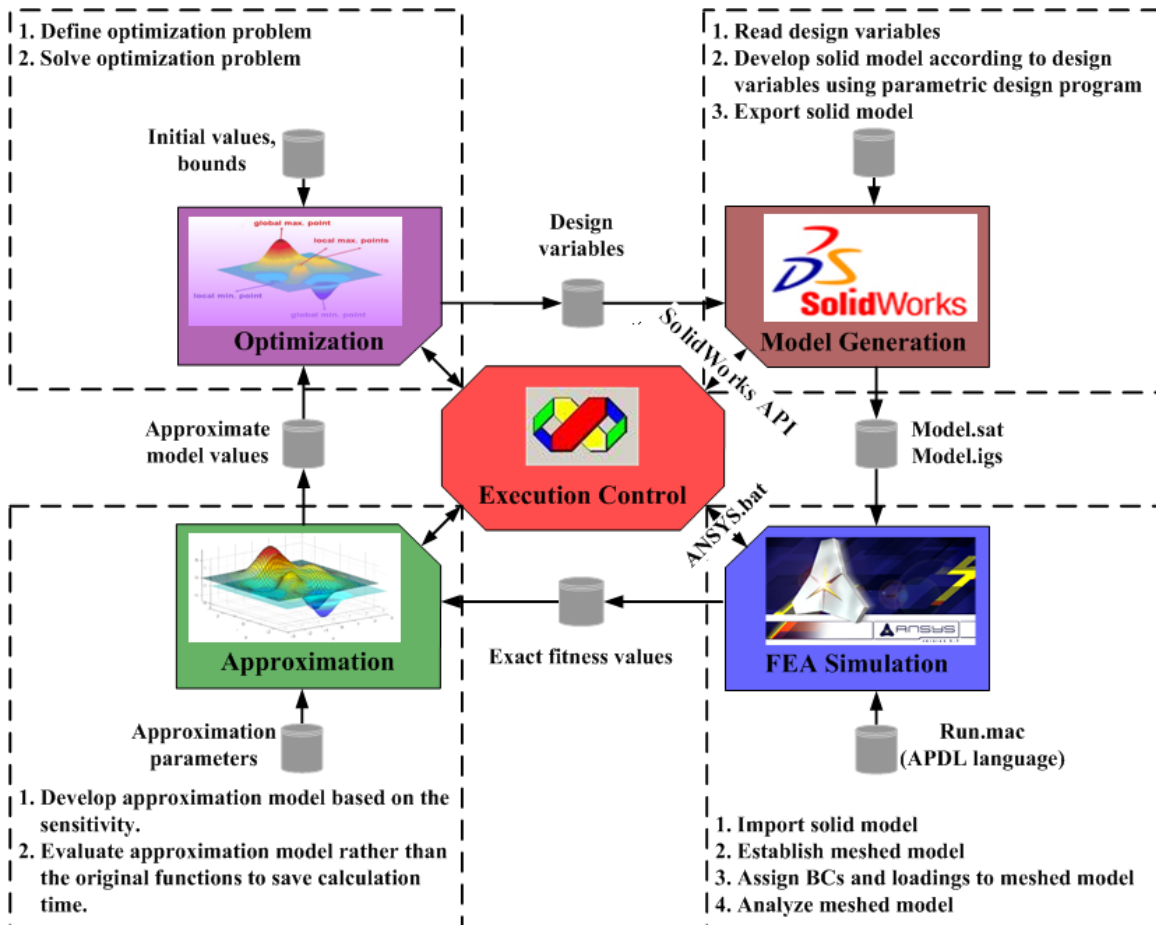
Figure 3-18 Flow chart of the optimization program

Chapter 4   Optimum Design of AOI Machine

This chapter aims at developing optimum design of the AOI machine structure. First, many modified base structures are proposed in order to reduce the deformation due to inertial force and increase the structural stiffness of the AOI machine base in both X-axis and Y-axis direction. Then a more suitable model is selected to carry out optimization. During the process of optimization, the finite element model will be calculated hundred or thousand times. Therefore, the finite element model of machine base is rebuilt by beam-shell to reduce the calculation time. By using this beam-shell model, optimum design variables for cross section can be received.

The inspection unit and X-axis beam are the moving parts during the inspection process, as shown in Fig. 3-10. The moving parts usually accelerate and decelerate substantially. The inertial force acting on the AOI machine is multiplied the mass of moving parts by 0.5g. Reducing the weight of moving parts can decrease the inertial force effectively while remain the acceleration of moving parts; or remain the same inertial force while increase the acceleration of the moving parts.

4.1 Modified Design for AOI Machine Base

The deformation of AOI machine base due to inertial force can be reduced by adding diagonal beams and oblique beams to the base. Five modified designs of AOI machine are proposed as shown in Fig. 4-1. The simulation results of modified design are listed in Table 4-1.
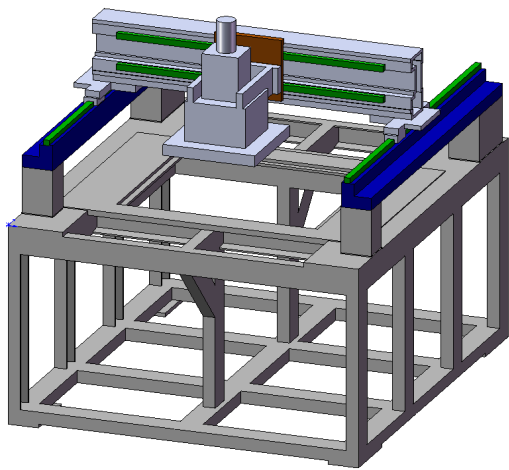
(a) Inner-oblique
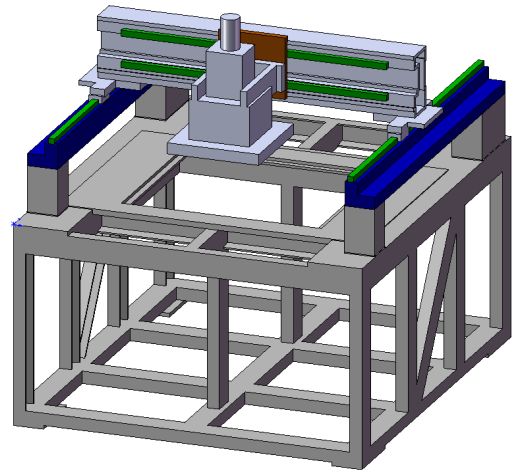
(b) LR-diagonal 1
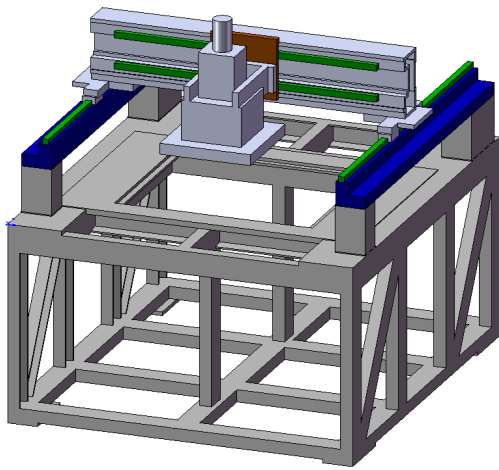
(c) LR-diagonal 2
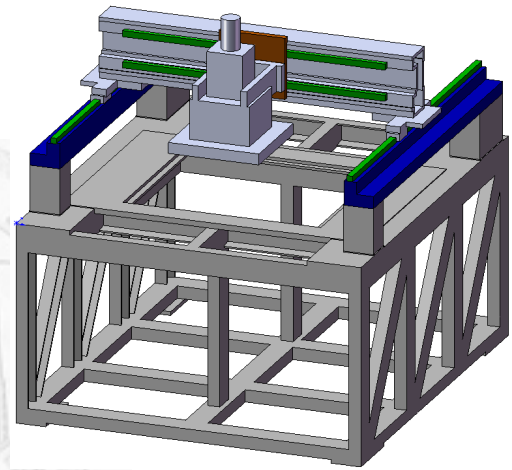
(d) LR-diagonal 3
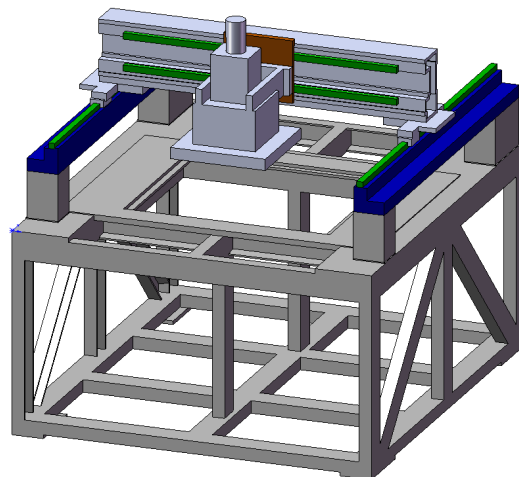
(e) LR-diagonal V

Figure 4-1 Modified design of AOI machine base

Table 4-1 Static analysis of modified machine base design

	Model	Volume changed (%)	Max def. of base (μm)	Def. changed (%)
Y-dir	Present model	---	7.07	---
	Inner-oblique	1.87	6.65	-5.94
	LR-diagonal 1	4.62	3.37	-52.33
	LR-diagonal 2	9.07	2.20	-68.88
	LR-diagonal 3	13.69	1.30	-81.61
	LR-diagonal V	3.20	1.27	-82.04

According to above analysis, conclusions can be made as following:

- The structural stiffness is weak if the base frame consists of vertical beams only.

- The deformation in Y-axis can be reduced 80% by adding diagonal beams on left side and right side of the base.

- The total volume of machine base is increased slightly.

4.2 Beam-Shell Finite Element Model for AOI Machine Base and Optimization

It takes hundred or even thousand times of analysis to finish structural optimization. In order to reduce total process time, ANSYS beam189 and shell93 are used to rebuild finite element model. In this way, a simplified model with loadings and boundary conditions is built, as shown in Fig. 4-2.
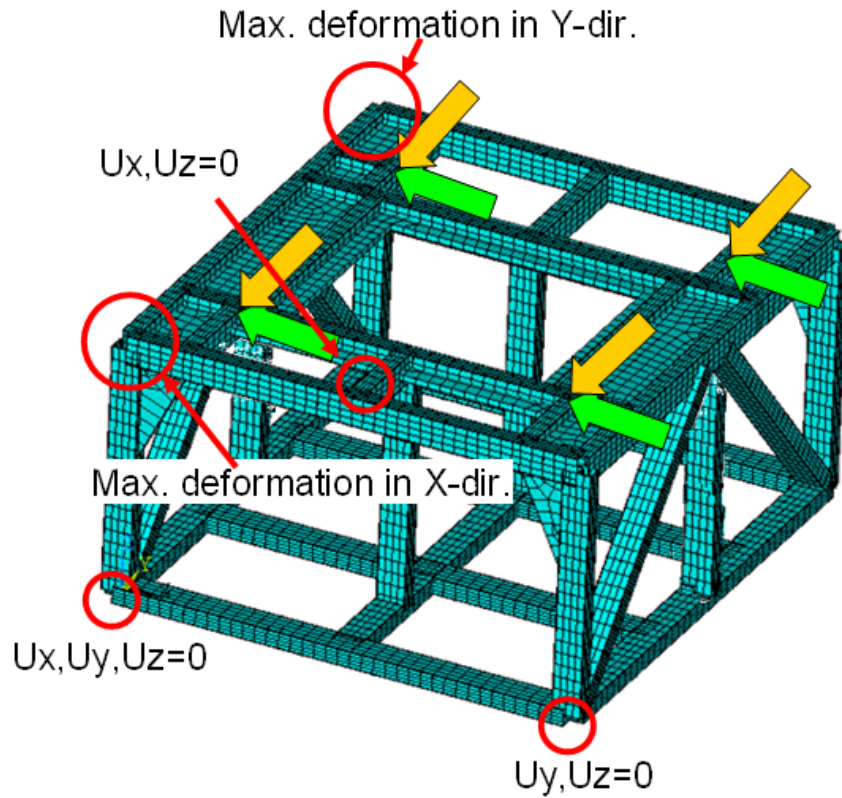
Figure 4-2 Simplified finite element model after modified design

This simplified finite element model has about 4,600 nodes and 28,000 D.O.F. and only takes 5 second to finish one analysis. Although this model can reduce calculation time effectively, it should also guarantee the accuracy of this model during static analysis. By comparing analysis results of two models, the error of simulation results between simplified beam-shell mesh model and solid mesh model is about 11%. Therefore, simplified model can be used to find optimum solution during optimization process, and it can also assure the accuracy of the simulation.

The numerical optimization problem can be written in the following form:

$$
\begin{aligned}
&\textit{Find } \vec{x}, \textit{Such that } F(\vec{x}) \rightarrow \min \\
&\textit{Subject to } g_i(\vec{x}) \le 0, i = 1,2,...,n_c
\end{aligned}
\tag{4-1}
$$

where $\vec{x}$ is the design vector, $F(\vec{x})$ is the objective function, $g_i(\vec{x})$ is the i_{th} constraint, and n_c is the number of constraints.

46

The optimization problem of the AOI machine is formulated by selecting three geometric parameters (x_i, $i = 1,2,3$) of the rectangle tube's cross section as the design variables. x_1, x_2 are the width and length of the rectangle tube, x_3 is the thickness of rectangle tube. The best modified design has diagonal-V steel structure in left side and right side of the base, as shown in Fig. 4-2. The constraints include the upper and lower limit of design variables and the displacement due to inertial force. According to the performance of modified design, the displacement due to inertial force is less than 0.5 times of original displacement in both X-axis and Y-axis direction, i.e. the structural stiffness in both X-axis and Y-axis direction is doubled. The optimization problem is formulated as:

$Find \ \vec{x}, \ Such \ that$

$F(\vec{x}) = V_b(\vec{x}) \rightarrow \min$

$Subject \ to$ (4-2)

$20mm < x_1 < 200mm; \ 0 < x_2 < x_1 \ ; 1.6mm < x_3 < 6mm;$

$U_x(\vec{x}) < 6\mu m \ (12\mu m \times 0.5) \ ; \ U_y(\vec{x}) < 3.5\mu m \ (7\mu m \times 0.5)$

where $U_x(\vec{x})$ is the maximum deformation in X direction, $U_y(\vec{x})$ is the maximum deformation in Y direction, $V_b(\vec{x})$ is the volume of base frame. After numerical searches of the structural optimization program, the optimum values are listed in Table 4-2. The ideal size for cross section of rectangle tube that calculated by optimum program is 67 x 67 x 1.6. By decreasing thickness in X-axis direction and increasing width to 67 mm, this design can strengthen the structural stiffness in X-axis. On the contrary, the structural stiffness decreased in Y-axis direction as the thickness and width both decreased. However, the structural stiffness decreased in y-axis can be improved even more by adopting LR-diagonal V base.

47

With this optimum design, the structural stiffness is doubled and total volume of base can be decreased 31.2% to 23,151cm^3 (original volume is 33,658cm^3). By using standard part of square tube 60 x 60 x 3.2, this structural stiffness of modified design, compared with original design, becomes 2.47 times in X-axis direction and 5.2 times in Y-axis direction, and 10.5% of the base weight is reduced.

Table 4-2 Design variables for the machine base

Parameter	Initial value	Optimum value
x_1	125 mm	66.9 mm
x_2	75 mm	66.9 mm
x_3	2.3 mm	1.6 mm
Ux	12.45 μm	6 μm
Uy	7.07 μm	1.92 μm
V_b	33,658 cm^3	23,151 cm^3

4.3 Modified and Optimum Design for X-axis Beam of AOI Machine

In order to decrease the weight of moving parts of AOI machine, selecting the total volume of X-axis beam as the object function. The optimization problem of the AOI machine is formulated by selecting four geometric parameters (x_i, $i = 1, 2, 3, 4$) of X-axis beam as the design variables. x_1, x_2, x_3 are the thicknesses in the cross-section of x-axis beam, x_4 is the side length of the square in the middle as shown in Fig. 4-3. The constraints follow the general aluminum extrusion limit for large-scale platform. The thickness of dimensions should not be less than 5mm. To avoid the geometrical error, three design variables should not be larger than 30mm simultaneously. Moreover, the effect of self-weight and inertial force in Y-axis direction should be taken into consideration as shown in Fig. 4-4. The behavior constraint is the deformation of lens which is a part of inspection unit. Therefore, this behavior constraint should not be

larger than the original deformation of inspection unit (45.6μm). The optimization problem is formulated as:

Find $\vec{x}$, Such that
$$F(\vec{x}) = V_{XB}(\vec{x}) \to \min$$
Subject to (4-3)
$$5mm < x_1, x_2, x_3 < 30mm \; ; \; 20mm < x_4 < 120mm$$
$$U_L(\vec{x}) < 45.6\mu m$$

where $U_L(\vec{x})$ is the deformation at the inspection lens tip, $V_{XB}(\vec{x})$ is the volume of the X-axis beam. After calculation by using optimization program, the optimum values are listed in Table 4-3. The iterative procedure is shown as Fig. 4-5. The total volume of X-axis beam can be decreased 26% to 6,464cm^3 (original volume is 8,753cm^3.)
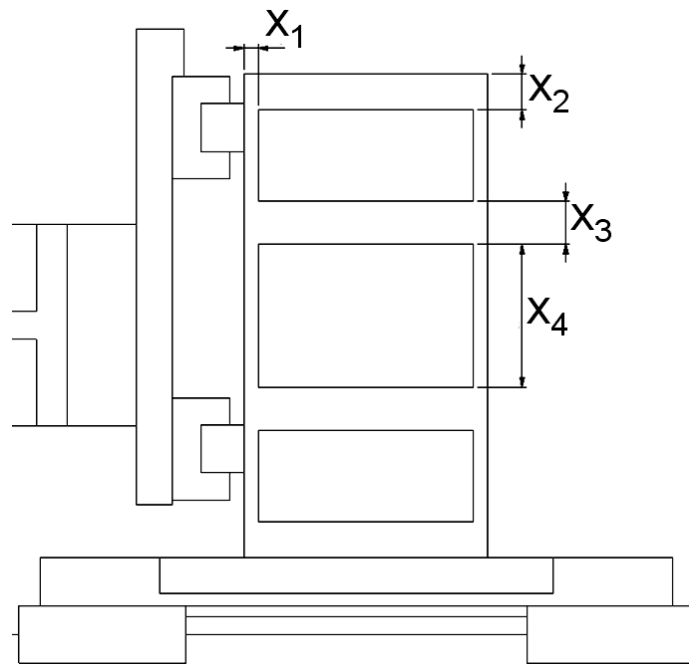
Figure 4-3 Parameters in the cross-section of X-axis beam
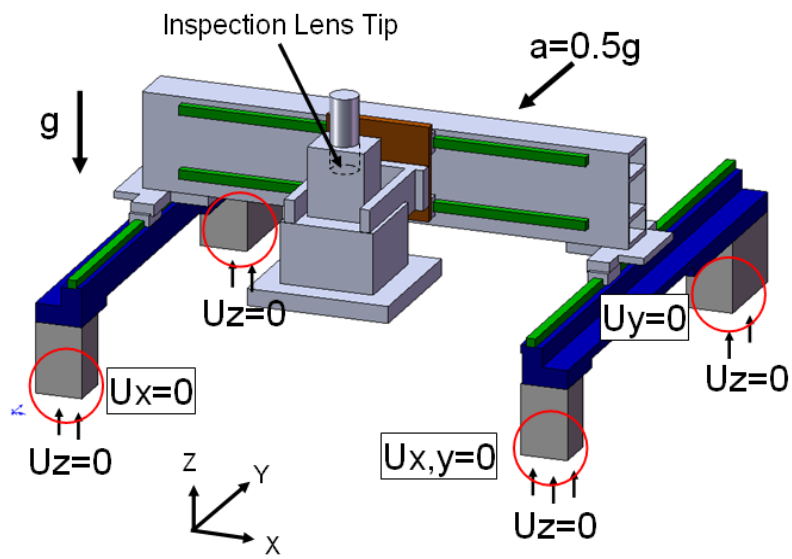
Figure 4-4 Loadings and boundary conditions of X-axis beam optimum design

Table 4-3 Light weight design variables for X-axis beam

Parameter	Initial value	Optimum value
x_1	6 mm	7.069 mm
x_2	18 mm	11.253 mm
x_3	15 mm	7.619 mm
x_4	60 mm	58.69 mm
V_{XB}	8,753 cm^3	6,464 cm^3
U_L	45.6 μm	45.6 μm
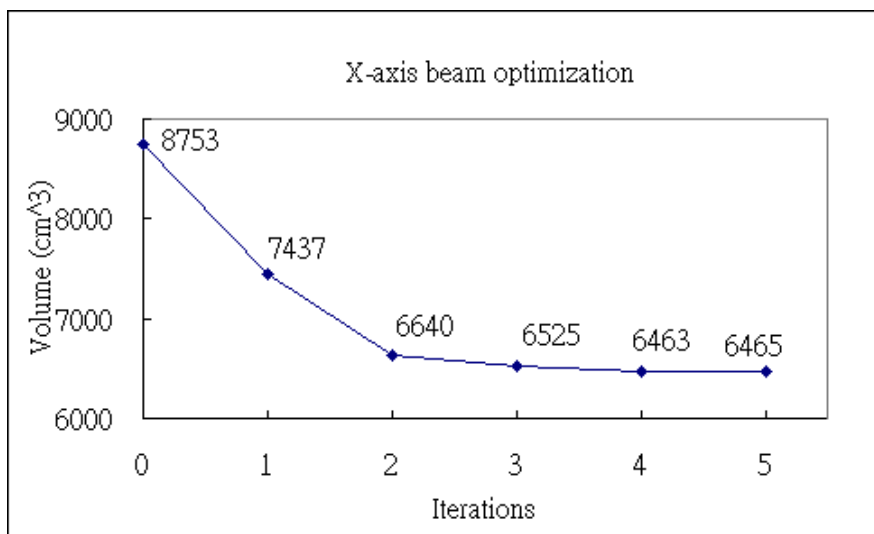
Figure 4-5 Iterative procedure of light weight optimum design

To reinforce the structural stiffness of AOI machine, selecting the deformation of lens at the same boundary condition and loadings as object function. The behavior constraint is the total volume of X-axis beam (8,753cm^3), while other settings remain the same. The optimization problem is formulated as:

Find $\vec{x}$, Such that
$$F(\vec{x}) = U_L(\vec{x}) \to \min$$
Subject to   (4-4)
$$5mm < x_1, x_2, x_3 < 30mm \; ; \; 20mm < x_4 < 120mm$$
$$V_{XB}(\vec{x}) < 8753cm^3$$

After calculation by using optimization program, the optimum values are listed in Table 4-4. The iterative procedure is shown in Fig. 4-6. The deformation of the lens can be decreased to 37.1μm (18.6% reduction).

Table 4-4 Structural reinforcement design variables for X-axis beam

Parameter	Initial value	Optimum value
x_1	6 mm	11.09 mm
x_2	18 mm	15.19 mm
x_3	15 mm	9.07 mm
x_4	60 mm	67.71 mm
V_{XB}	8,753 cm^3	8,753 cm^3
U_L	45.6 μm	37.1μm
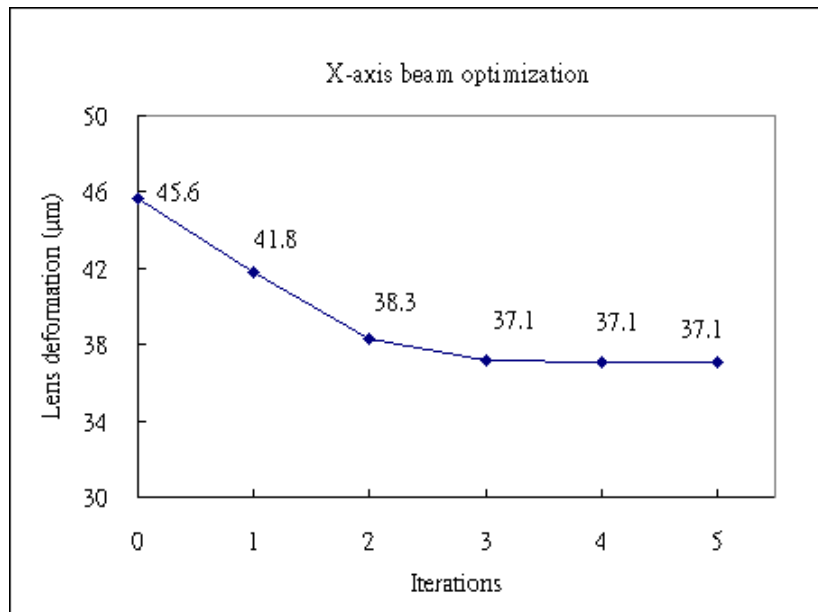
Figure 4-6 Iterative procedure of structural reinforcement optimum design

After numerical searches of the structural optimization, 26% of the x-axis beam weight can be reduced when the deformation of lens remains the same, or 19% of the lens deformation is reduced meanwhile the volume remains the same. Hence, the inspection unit can be moved with a higher acceleration, then the AOI machine can use linear motor with lower power as actuator, or a better image quality can also be acquired during the inspection process.

Chapter 5 Thermal Compensation Design of AOI

Machine

In the chapter, the temperature distribution of AOI machine under the temperature distribution becoming steady state is detected by an infrared thermometer and the thermal couple. After the experiment results are obtained, the temperature distribution can be very closely simulated in ANSYS. Since the temperature distribution is re-performed in ANSYS, the thermal deformation analysis can also be executed. According to the result of thermal deformation analysis, a thermal compensation design is proposed to compensate the thermal error of the AOI machine.

5.1 Temperature Distribution Analysis

For detecting the temperature distribution of AOI machine under the temperature distribution become steady state, the infrared thermometer is used. It measures the temperature using blackbody radiation emitted from detected object that the wave length range of this radiation is about 0.7μm ~ 1mm (infrared), as shown in Fig. 5-1. Therefore infrared thermometer can measure the temperature from a distance (non-contact). By knowing the surface emissivity and energy emitted by the detected object, the temperature of object can be determined.
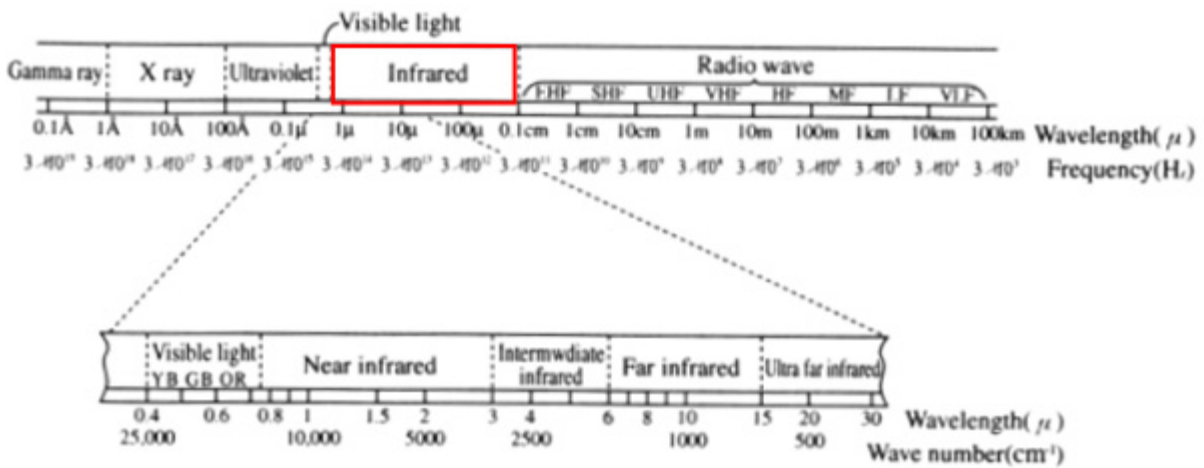
Figure 5-1 Infrared position on spectrum [21]

Although the infrared thermometer is detecting the energy from the object surface, the energy is not only emitted from object. The energy is sum of emission, reflection and transmission by the surface, as shown in Fig. 5-2. So that not all surfaces are suitable for infrared thermometer measurement, such as: transmission with infrared, shining surface (metal) and other surface with high reflection. Adding tapes with knowing emissivity can solve this problem and get accuracy result.

If transmission=0,
W = Emission + Reflection
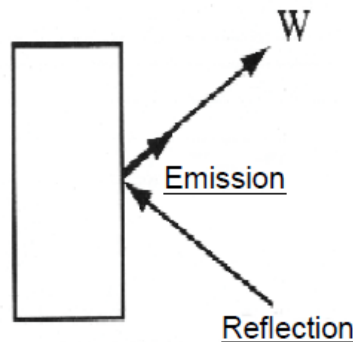
Figure 5-2 The energy is sum of emission, reflection and transmission [21]

The arrangements of temperature distribution experiment consist of the infrared thermometer fixed by a tripod and measuring the X-axis beam of AOI machine, as

shown as Fig. 5-3 and 5-4. After machine switch on, the environment temperature is

25.3℃. The experiment is measured until the temperature stabilized, spent a total of 5

hours. The initial and final temperature distributions are shown as Fig. 5-5 and 5-6.

Figure 5-3 The arrangement of temperature distribution experiment
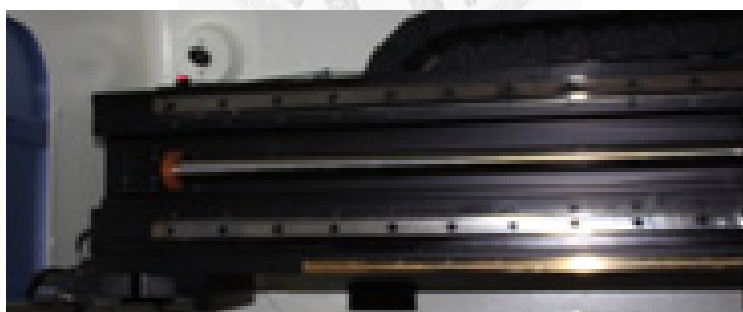
Figure 5-4 Measuring the X-axis beam of AOI machine
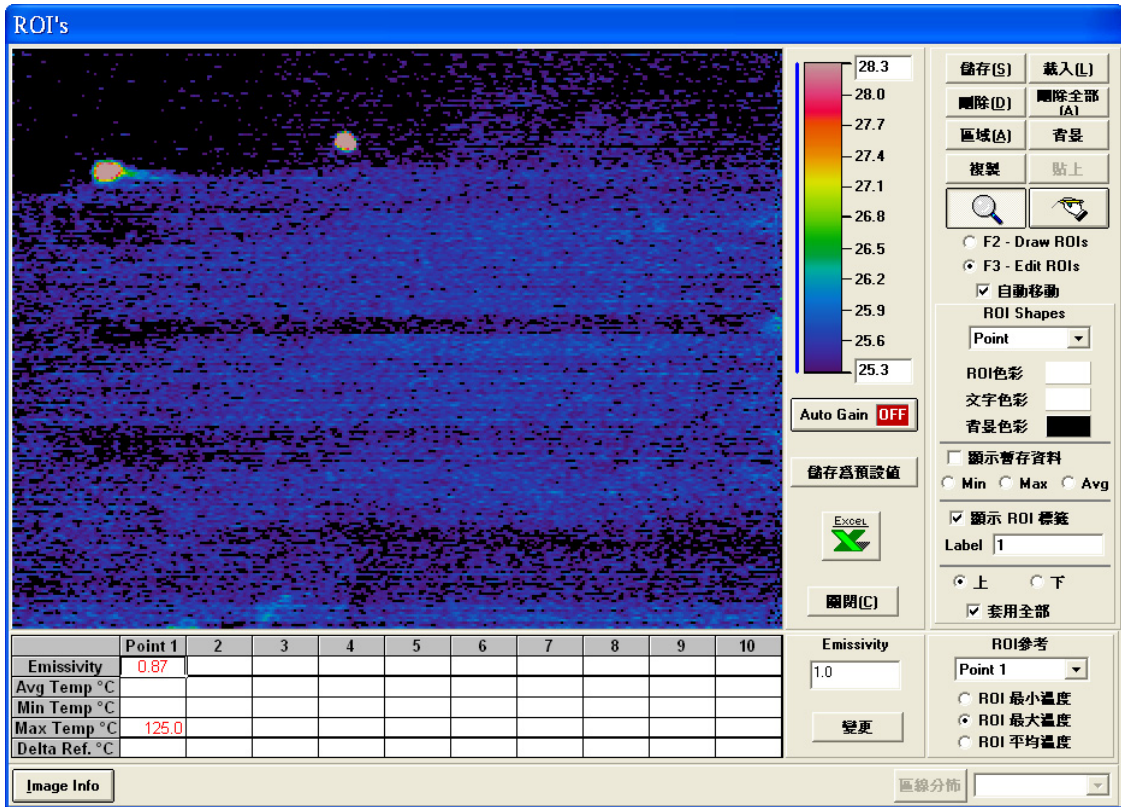
Figure 5-5 Initial temperature distribution
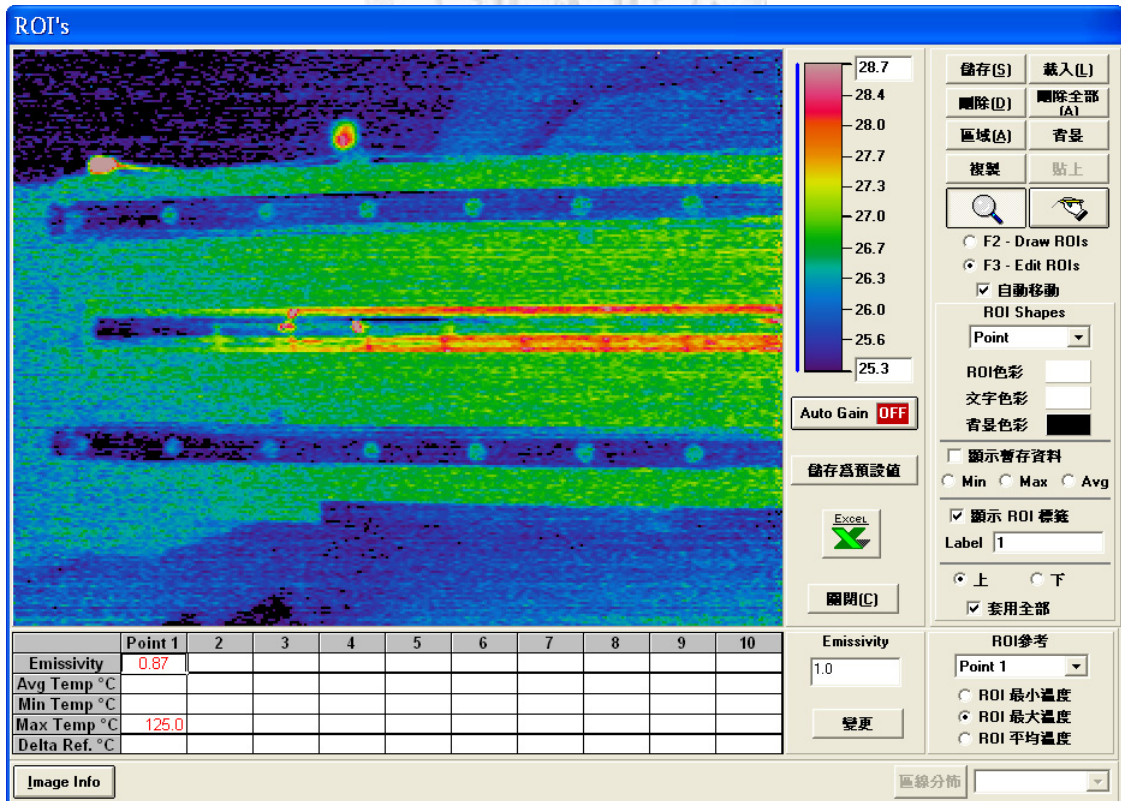
Figure 5-6 Final temperature distribution

As the results show that the temperature of X-axis beam ranges from 26.2℃ to 27.1℃. Note that there are some red color regions on linear motor stator in Fig. 5-6. In general, red region means higher temperature but the linear motor stator has shining surface which is not suitable to measure temperature by an infrared thermometer because of the reflection. Here the thermal couple is used to measure the temperature of stator. The results show that the temperature of linear motor stator ranges from 27.5℃ to 33.5℃.

After the experiment results are obtained, the temperature distribution can be very closely simulated in ANSYS. The boundary conditions and the result are shown in Fig. 5-7 and 5-8. The temperature of the X-axis beam ranges from 26.3℃ to 27.3℃. For verifying the result from FEM and experiment, a series of temperature numerical at X-axis beam from end to mid are captured, as shown as Fig. 5-9. In this figure, it shows that the FEM result is very close to experiment result.
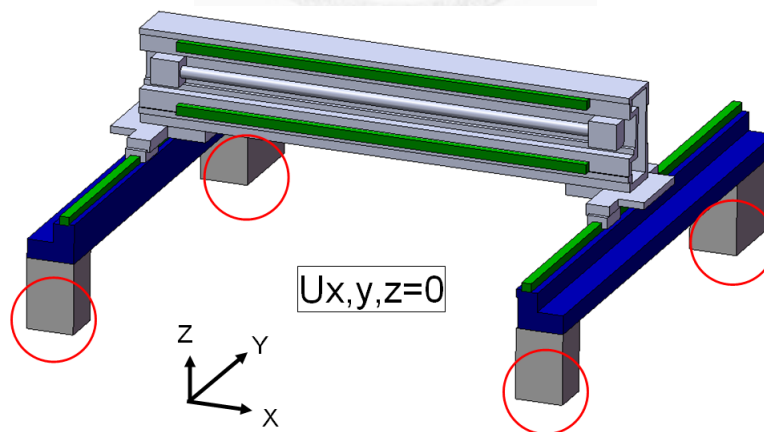
Figure 5-7 The boundary conditions of temperature distribution analysis
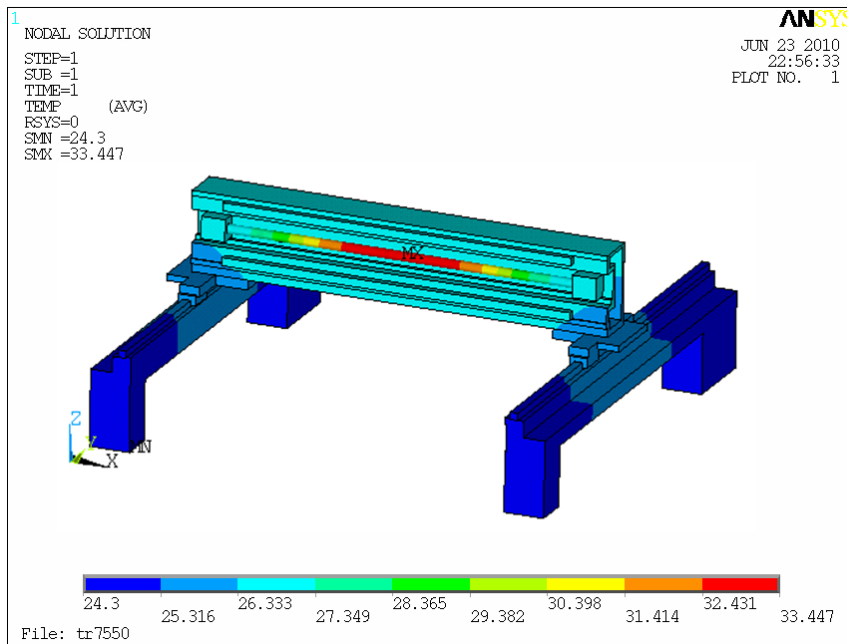
Figure 5-8 The result of temperature distribution analysis by ANSYS
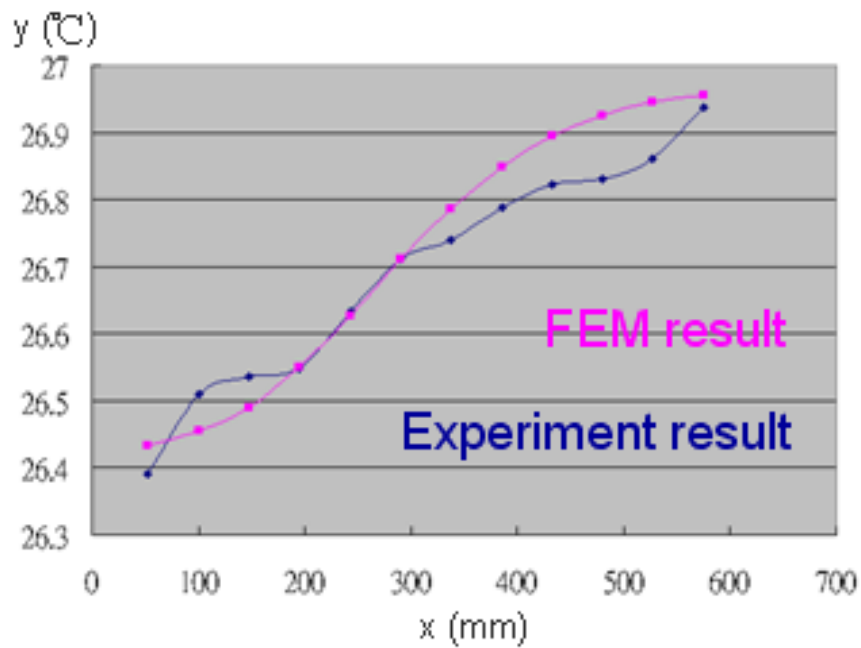
Figure 5-9 Compare temperature distribution result of FEM with experiment

5.2 Thermal Deformation Analysis

Since the temperature distribution is re-performed in ANSYS, the thermal deformation analysis can also be executed. Noting that the coefficients of thermal

expansion of steel and aluminum are 23.6 and 11.5μm/m-°C separately. After the thermal deformation analysis, the thermal deformation result can be obtained, as shown as Fig. 5-10. The analyzed maximum deformation of AOI machine is 26.23μm. Simultaneously, the components of the maximum related deformations of X-axis beam in X, Y and Z direction are 41.16μm, 17.44μm and 13.61μm respectively, as shown in Fig. 5-11 to 5-13.
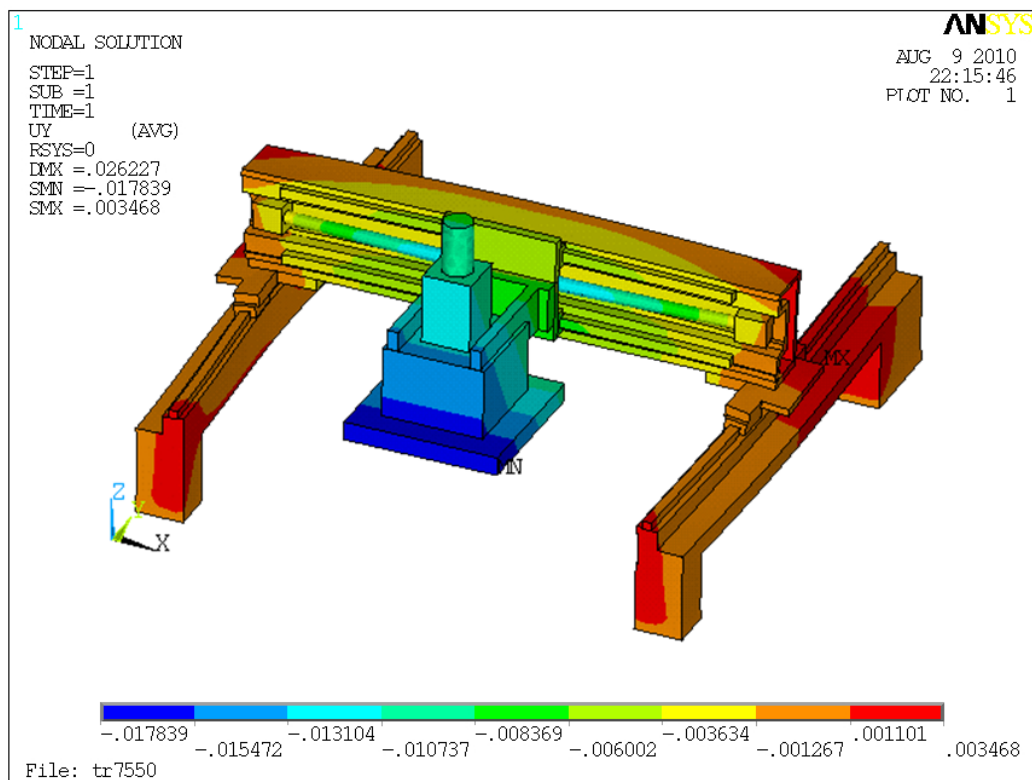
Figure 5-10 The thermal deformation of AOI machine in Y-dir
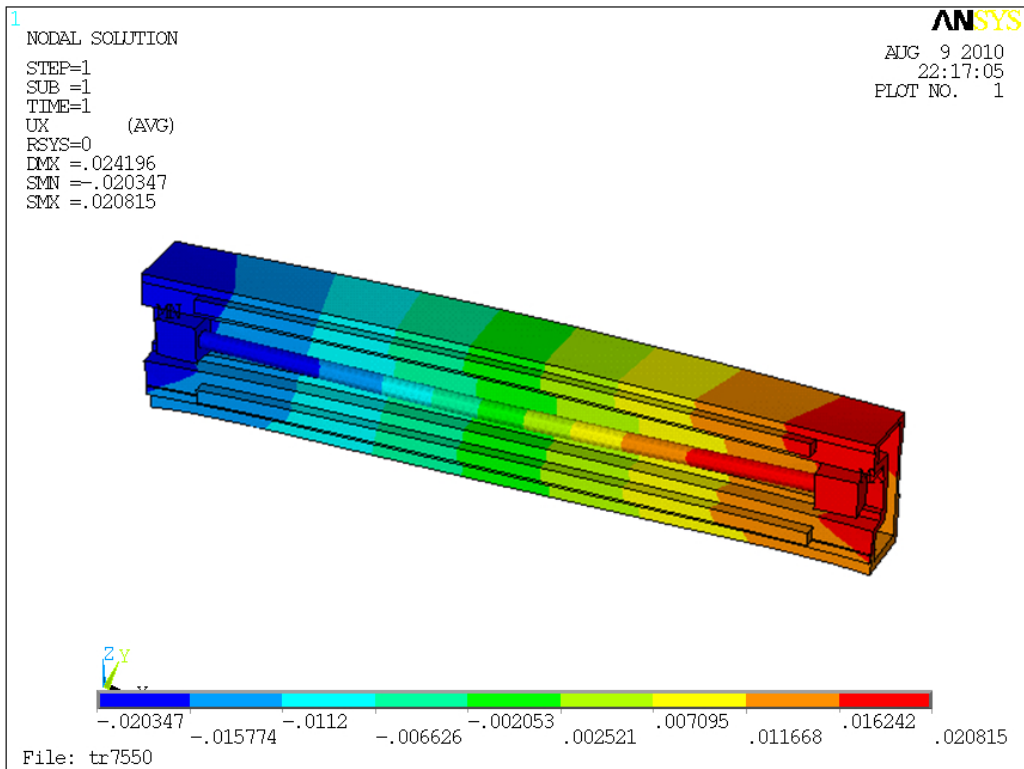
Figure 5-11 The thermal deformation of X-axis beam in X-dir
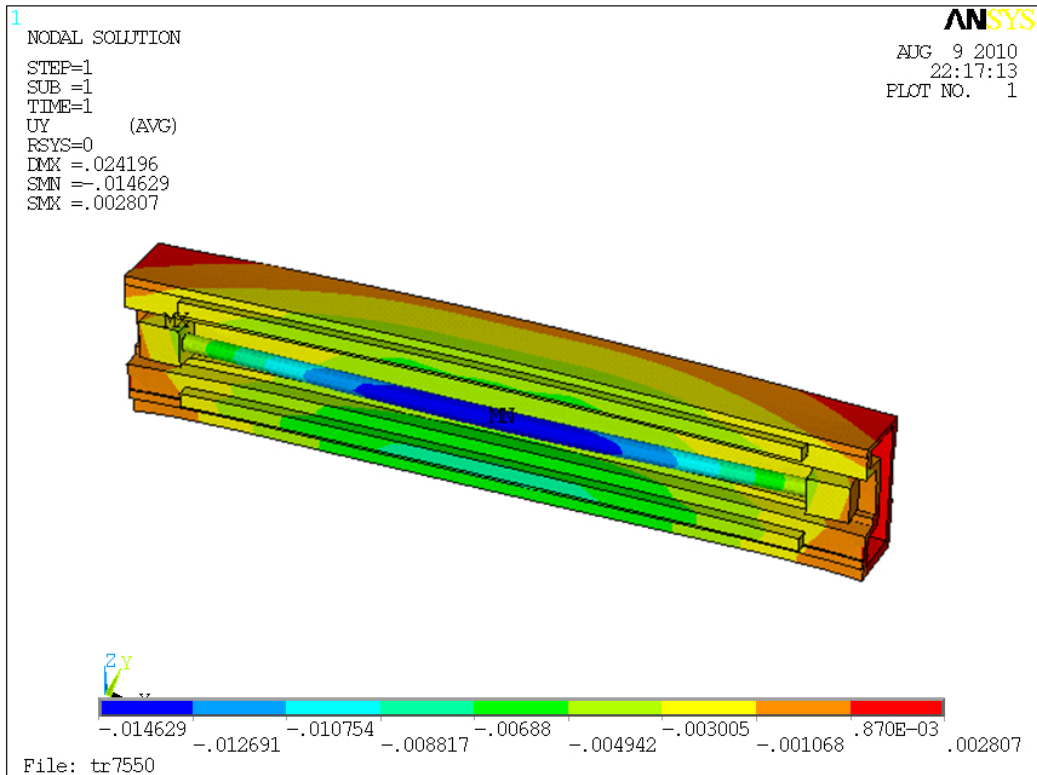
Figure 5-12 The thermal deformation of X-axis beam in Y-dir
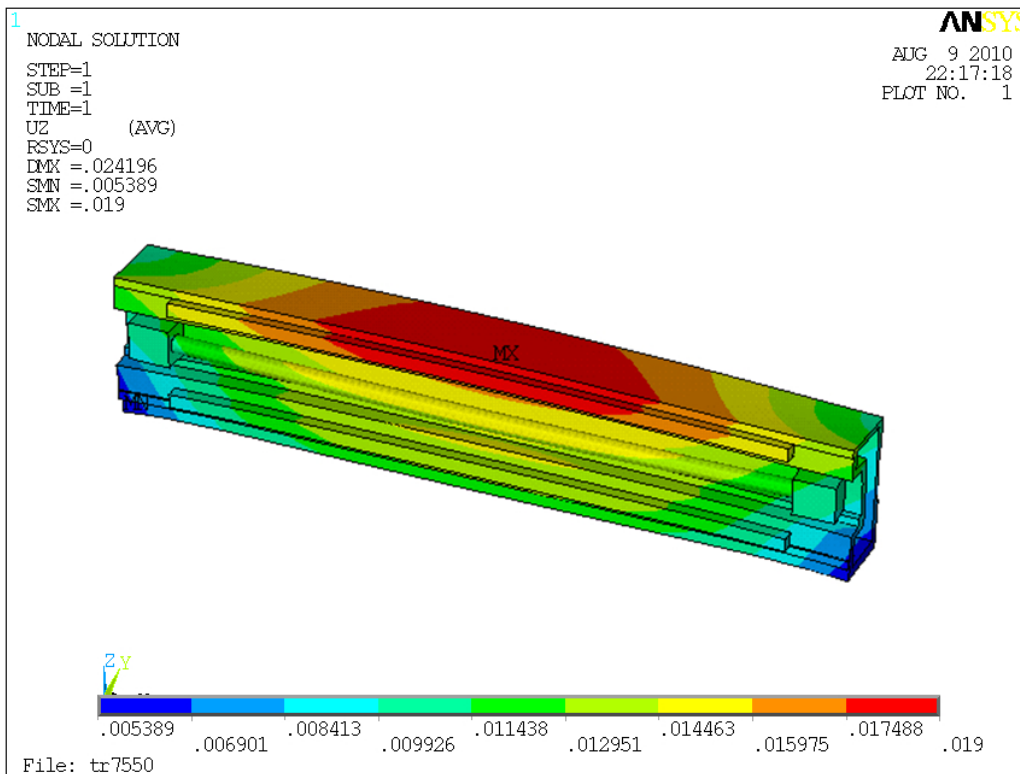
Figure 5-13 The thermal deformation of X-axis beam in Z-dir

Noting that the thermal deformations of X-axis beam in both X and Z-direction are similarly uniform extension in their direction, but not the same in Y-direction. The Y-direction thermal deformation of the X-axis beam is generated by the mismatch expansion, which is the coefficient of thermal expansion multiplied by average temperature variation, between X-axis beam and linear motor stator.

5.3 Thermal Compensation Design

Because of the CTE and temperature variation are different between X-axis beam and linear motor stator, as shown in Fig. 5-14, there is bending occurred. In the above analysis, the elongations of both X-axis beam and linear motor stator can be probably estimated as Eq. 5-1.

61

$$
\begin{cases}
L_{Xb} = L_0 + \alpha_{Xb} \times \varDelta T_{Xb} \times L_0 \\
L_{LMs} = L_0 + \alpha_{LMs} \times \varDelta T_{LMs} \times L_0
\end{cases}
\tag{5-1}
$$

where α_{Xb} and α_{LMs} are the thermal expansion coefficients of X-axis beam and linear motor stator, $\varDelta T_{Xb}$ and $\varDelta T_{LMs}$ are the average temperature variation of X-axis beam and linear motor stator, L_0 is the original length of linear motor stator, L_{Xb} and L_{LMs} are the lengths by thermal expansion. The elongations of X-axis beam and LM stator are 35.4μm and 59.8μm separately. Because of the mismatch of elongations, the structure of X-axis beam bends like an arc opening upward.
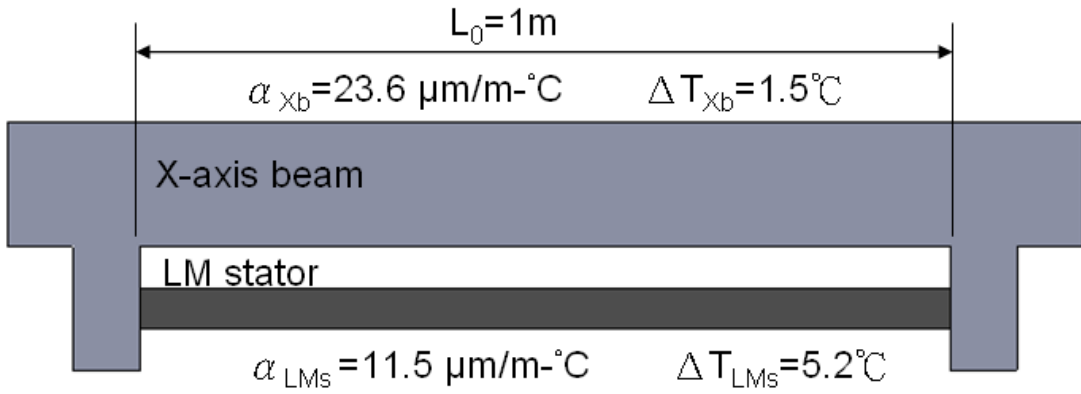
Figure 5-14 X-axis beam schematic diagram in thermal expansion

The bending structure makes the inspection unit moving along the X-axis beam but producing Y-direction displacement. A thermal compensation design concept is proposed to compensate this thermal error, as shown in Fig. 5-15.
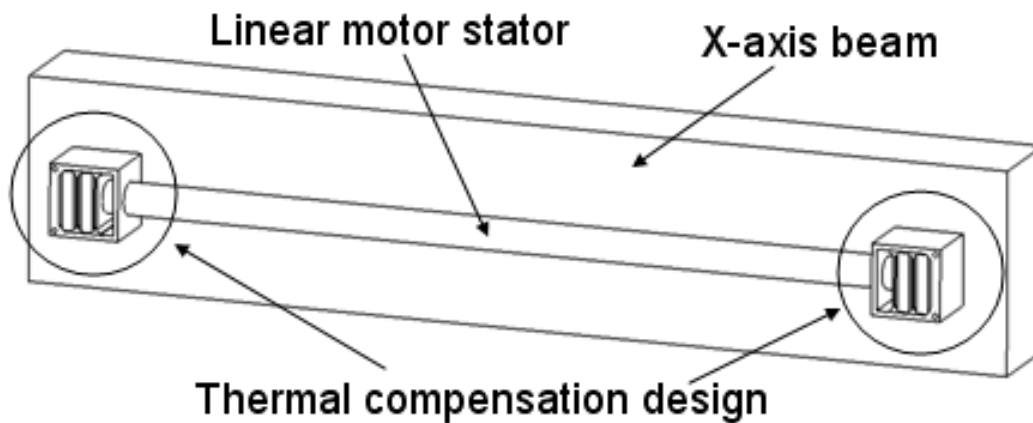
Figure 5-15 Thermal compensation design concept

This thermal compensation designs connect the ends of linear motor stator and the X-axis beam. They support the stator and provide the thermal compensation at the same time. In the detail view of the design, it has a box with a hole and two bevel surfaces with the same degree. It also has several plates with rectangle-shaped and I-shaped cross sections. The plates also have the bevel surfaces and the same degree with the box, as shown in Fig. 5-16. Noting that their bevel angles are connected sequentially and the degree angle $= \theta$.
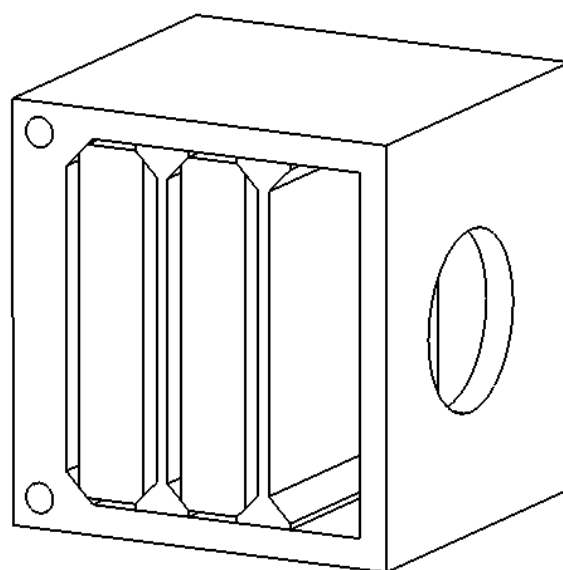
Figure 5-16 Thermal compensation design concept

Local view of this design, a box and a rectangle-shaped plate are selected, as shown in Fig. 5-17. They are connected by the bevel surface. Different materials are used between box and plate with CTE α_A and α_B. If the temperature of the design rises ΔT_{box} °C, the heights of box and plate are separately formulated as:

$$\begin{cases} H_A = H_0 + \alpha_A \times \Delta T_{box} \times H_0 \\ H_B = H_0 + \alpha_B \times \Delta T_{box} \times H_0 \end{cases} \tag{5-2}$$

where H_A and H_B mean the heights of the box and plate with material A and B after the temperature rising ΔT_{box} °C. Since $\alpha_A \neq \alpha_B$, the elongations are not the same. For the bevel surfaces keeping connected, there is relative movement between these two parts by sliding in the bevel surfaces.
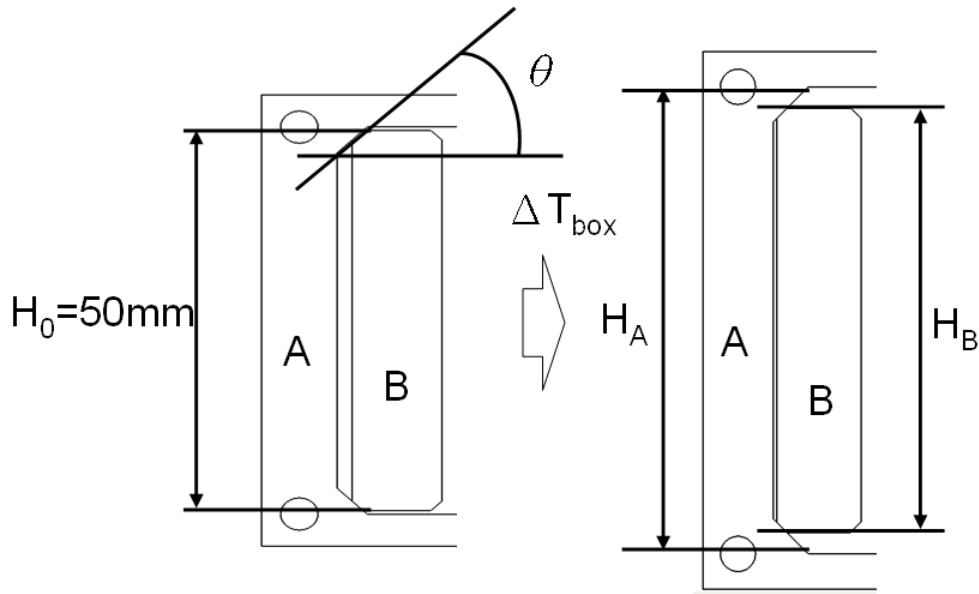
Figure 5-17 Local view of the design and principle

As the (H_A - H_B) and (L_{LMs} - L_{Xb}) are known, the degree of the bevel surfaces θ can be determined as Eq. 5-3 and Fig. 5-18. Considering the multi-plates exist in the box at the same time.
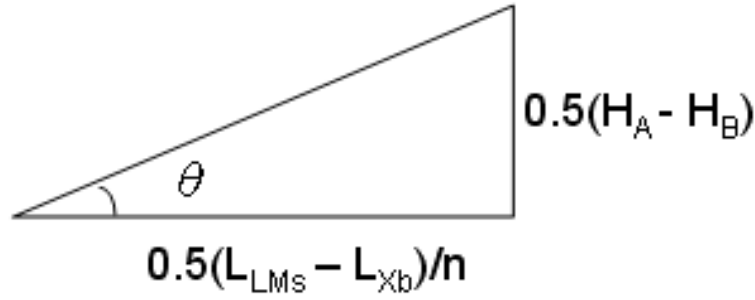
Figure 5-18 The relationship of θ and legs of right triangle

$$\tan\theta = \frac{H_A - H_B}{(L_{LMs} - L_{Xb})/n} \tag{5-3}$$

Substitute by Eq. 5-1 and 5-2:

$$\tan\theta = \frac{\alpha_A \times \Delta T_{box} \times H_0 - \alpha_B \times \Delta T_{box} \times H_0}{\alpha_{LMs} \times \Delta T_{LMs} \times \dfrac{L_0}{n} - \alpha_{Xb} \times \Delta T_{Xb} \times \dfrac{L_0}{n}}$$

$$= \frac{H_0 \times n}{L_0} \times \frac{(\alpha_A - \alpha_B) \times \Delta T_{box}}{\alpha_{LMs} \times \Delta T_{LMs} - \alpha_{Xb} \times \Delta T_{Xb}} \tag{5-4}$$

where the n means the number of plates a box has. Assume the material of box and I-shaped plate is aluminum and rectangle-shaped plate is invar. The CTE of the invar is very small (1.2 μm/m-°C). The Eq. 5-4 can be expressed as Eq. 5-5.

$$\tan\theta = \frac{H_0 \times n}{L_0} \times \frac{22.4 \times \Delta T_{bar}}{11.5 \times \Delta T_{LMs} - 23.6 \times \Delta T_{Xb}} \tag{5-5}$$

According to this equation and the said experiment result ($\Delta T_{box} = 1.6$ °C, $\Delta T_{LMs} = 5.2$ °C, $\Delta T_{Xb} = 1.5$ °C), the value of the θ can be determined as $\theta = 4.2°$ with one plate in box; the value of the θ can be determined as $\theta = 8.36°$ with two plates in box; the value of the θ can be determined as $\theta = 16.37°$ with four plates in box and so on. Considering the self-locking, the coefficient of friction between plain bearing with thin film lubricated is about 0.08. The friction angle is about $4.6°$.

Therefore the self-locking will not be occurred if at least two plates are used. The thermal compensation design schematic is shown as Fig. 5-19.
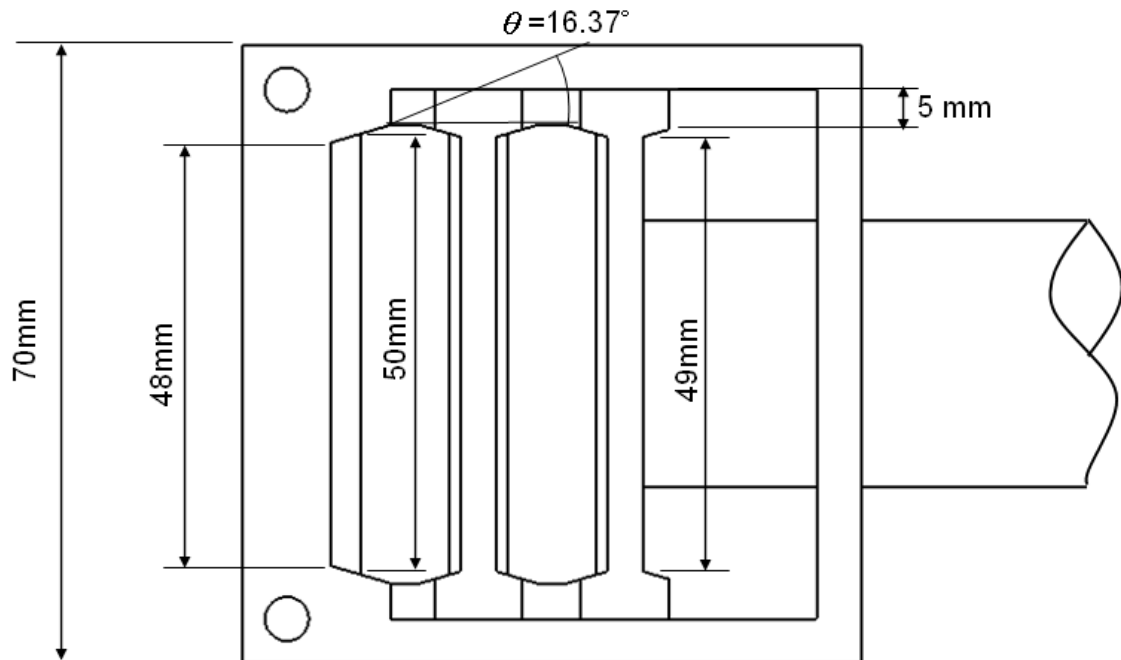
Figure 5-19 Thermal compensation design schematic diagram with four plates

Chapter 6   Conclusions and Perspectives

6.1 Conclusions

This paper studies the FEM analysis, optimum design and thermal error of the AOI machine structure. The conclusions in this paper can be summarized as follows:

1. The model analysis is correct and is verified by modal test. The result of modal test of the AOI machine is close to that of the modal analysis in natural frequencies and mode shapes. The maximum error of natural frequency is about 9.6%.

2. An integrated program is developed to decrease the weight of the AOI machine. The program is composed of model generation with SolidWorks API, FEA simulation with ANSYS, response approximation and numerical optimization. The program can automatically update model parameters, analyze structural responses and search the optimum solution for design parameters. Both structural optimizations of the AOI machine are carried out. For the optimum design of the AOI machine base, the base weight is reduced by 31.2% and the structural stiffness of the base is doubled. For optimum design of moving parts of the AOI machine, 25% of the x-axis beam weight is reduced, and the structural stiffness is almost the same.

3. The temperature distribution analysis of the AOI machine is executed according to the experimental result. The temperature distribution experiment results of AOI machine is measured with IR thermometer and thermal couple. The temperature ranges between 26.3°C to 27.3°C at X-axis beam and 27.5°

C to 33.5°C at linear motor stator in environment temperature 25.3°C. For adapting the results of thermal distribution experiment, the thermal distribution analysis is proposed. The temperature ranges between 26.2°C to 27.1°C at X-axis beam. Therefore, the response of the temperature distribution analysis can stand for the actual characteristic of the AOI machine.

4. A thermal compensation design is proposed to reduce the thermal deformation of the AOI machine. According to the thermal deformation analysis based on the temperature distribution analysis, the thermal deformation is large. For example, the analyzed maximum deformation of AOI machine is 40.74μm. Also, the components of the maximum deformations of X-axis beam in X, Y and Z direction are 40.55μm, 17.02μm and 8.54μm respectively. The thermal deformation of the AOI machine is generated by the coefficient of thermal expansion mismatch between X-axis beam and linear motor stator. In order to reduce the deformation, the thermal compensation design is proposed and it can compensate relative large deformation in a small structure.

6.2 Perspectives

This paper studies the FEM analysis, optimum design and thermal error of the AOI machine structure. But there are still some contents worth developing and improving in the future, as follows:

1. In the modal analysis and modal test, this paper compares two results of each other. It shows that the modal analysis is correct and is verified by modal test.

However, these results cannot predict actual situation during operation because there are many equipments and machine case mounted on this machine structure. These equipments and machine case will have great reflection on the response of the machine structure.

2. According to the optimum design result of the machine base, it is suggested that the channel steel should be replaced by the square tube steel. However, if square tube steel was used, the wiring would be a problem. Therefore, channel steel is still used.

3. Although the optimum designs of the AOI machine are completed, some unconsidered design criterions should be established. They are about the allowable toleration of inspection unit deformation and the allowable deflection of machine structure under full loading. According these criterions, a better design of AOI machine structure can be received

References

[1] J. Muller, J. Klein, J. Rayho, "In-process verification of MLC substrates," Microelectronics Reliability, Vol.43, pp.371-375, 2003.

[2] K. C. Fan and C. Hsu, "Strategic planning of developing automatic optical inspection (AOI) technologies in Taiwan," J. of Physics—Conference Series, Vol.13, pp.394-397, 2005.

[3] J. J. Wu, "Finite element modeling and experimental modal testing of a three-dimensional framework," International Journal of Mechanical Sciences, Vol. 46, pp. 1245–1266, 2004.

[4] Jochen M. Rieber and David G. Taylor, "Integrated control system and mechanical design of a compliant two-axes mechanism," Mechatronics, Vol. 14, pp.1069-1087, 2004.

[5] D.R. Griffiths and J.C. Miles, "Determining the optimal cross-section of beams," Advanced Engineering Informatics, Vol. 17, pp. 59-76, 2003.

[6] R. N. Mathivanan, R. S. Sharma, Dr V P Raghupathy, "Dynamic analysis and optimization of machine base for crankshaft pin milling machine," IE(I) Journal–MC, vol. 88, 2007.

[7] J. Gomand, R. Bearee, X. Kestelyn, P. J. Barre, "Physical dynamic modeling and systematic control structure design of a double linear drive moving gantry stage industrial robot," 2007 European Conference on Power Electronics and Applications, 2007.

[8] Ling Zhao, Wu-yi Chen, Jian-feng Ma, Yong-bin Yang, "Structural bionic design

and experimental verification of a machine tool column," Journal of Bionic Engineering Supply. pp. 46-52, 2008.

[9] Soon Chul Jung, Jae Euna Lee, Seuna Hwan Chang, "Design of inspecting machine for next generation LCD glass panel with high modulus carbon/eproxy composites," Composite Structures, Vol. 66, pp. 439-447, 2004.

[10] Ju Ho Kim, Jae Eung Lee, Seung Hwan Chang, "Robust design of microfactory elements with high stiffness and high damping characteristics using foam-composite sandwich structures," Composite Structures, Vol. 86, pp. 220-226, 2008.

[11] Sun-Kyu Lee, Jae-Heung Yoo, Moon-Su Yang, "Effect of thermal deformation on machine tool slide guide motion," Tribology International, Vol. 36, pp. 41-47, 2003.

[12] E. Creighton, A. Honegger, A. Tulsian, D. Mukhopadhyay, "Analysis of thermal errors in a high-speed micro-milling spindle," International Journal of Machine Tools & Manufacture, Vol. 50, pp. 386-393, 2010.

[13] A. Gelman, E. Maliah, "Mechanism for passive thermal compensation in harsh environment," Proc. of SPIE, Vol. 6715, pp. 671506-1-671506-12, 2007.

[14] Mark Stern, Charles Airesman, Vijay Pandit, all of Cumberland, Md., "Load cell temperature compensation system," United States Patent No. 4543837, 1985.

[15] Michael J. O'Brien, William B. Smith, Both of Rochester, N. Y., "Method and apparatus for combined active and passive athermalization of an optical assembly," United States Patent No. 5313333, 1994.

[16] Donald McCrary, Orlando, Fla., "Thermal loading retainer," United States Patent

No.6108145, 1999.

[17] A. Yunus, Heat transfer - a practical approach, McGraw-Hill, pp. 466-475, 1997.

[18] J. M. Gere, Mechanics of materials-fifth edition, Brooks/Cole, pp. 271-302, 2001.

[19] ANSYS® Academic Research, Release 10, Help System, ANSYS, Inc.

[20] Polytec, http://www.polytec.com/

[21] Nippon Avionics CO.,LTD., http://www.avio.co.jp/

Appendix A Parametric Solid Model Design by SolidWorks

A.1 SolidWorks API by Visual Basic of MicroSoft Visual Studio 2005

Based on the parametric design and feature tree, SolidWorks utilizes an approach based on parametric feature to create models and assemblies. For any model from SolidWorks, two executables (EXE files) are developed to update the model parameters and export ACIS SAT model for FEM software. They are controlled by command line arguments. Designers can update parameter by command:

"SW_PChange <part_name.sldprt> <parameter_name> <value>"

Export ACIS model by command:

"SW_OutputSAT <part_name.sldprt> <part_name.sat>"

The constructing procedure of the executables is described as follows:

1. Open Visual Studio 2005.

2. Select <File> and press <New Project>.

3. Choose <Visual Basic> in <Project types>, and choose <Console Application> in <Templates>. The project is named <SW_PChange> or <SW_OutputSAT>. Then press <OK>.

4. For the connection between SolidWorks and VB, the reference should be added. Choose <Project> <Add Reference…>, and choose <SldWorks 2007 Type Library> in page <COM>, and press <OK>.

5. Write the content. (See sec.A.2)

6. After finish the code and press <Start Debugging>, SW_PChange.exe or SW_OutputSAT.exe and Interop.SldWorks.dll can be found in <Project>\<Project_name>\<Project_name>\bin\Debug direction.

7. Open SolidWorks, open SolidWorks CAD file *.sldprt, and run the executables with command line. For example:

SW_PChange.exe box.sldprt length@Sketch1 60

SW_OutputSAT.exe box.sldprt box.sat

A.2 Code Description

The codes of SW_PChange.exe and SW_OutputSAT.exe are interpreted as follow:

SW_PChange.exe

```vb
Module Module1
    Sub Main()
        Dim Args() As String
'Define a matrix
        Args = Split(Command$, " ")
'Split the command line behind the *.exe by space. Then assign the arguments to matrix Args().
'ex. A.exe a bb ccc
'→ Args(0)=a, Args(1)=bb, Args(2)=ccc
        If UBound(Args) = 2 Then
'It is expect that thecommand line is <part_name.sldprt> <parameter_name> <value>, so that if the
number of arguments is 3 then the follows will be done.
            Dim swApp As New SldWorks.SldWorks
            swApp.Visible = True
'Declare the swApp as an object of SolidWorks.
            Dim Model As SldWorks.ModelDoc2 = swApp.OpenDoc6(Args(0), 1,
0, "", 0, 0)
'Open the sldprt file as the string of Args(0), then declare it as Model.
```

```
                    Model.Parameter(Args(1)).SystemValue = Args(2) / 1000
'Set the value of parameter name Args(1) is the value in Args(2)
                Model.EditRebuild3()
                Model.Save()
'Rebuild and save the model.
        Else
                Console.Write("SW_PChange <part_name.sldprt>
<parameter_name> <value>")
'If the number of the arguments behind *.exe is not 3, the string will be output to remind user.
        End If
        GC.Collect()
'release memory
    End Sub
End Module
```

SW_OutputSAT.exe

```
Module Module1
    Sub Main()
        Dim Args() As String
        Args = Split(Command$, " ")
        If UBound(Args) = 1 Then
            Dim swApp As New SldWorks.SldWorks
            swApp.Visible = True
            Dim Model As SldWorks.ModelDoc2 = swApp.OpenDoc6(Args(0), 1,
0, "", 0, 0)
            Model.SaveAs(My.Application.Info.DirectoryPath & "\" &
Args(1))
        Else
            Console.Write("SW_PChange <part_name.sldprt>
<part_name.sat")
        End If
        GC.Collect()
    End Sub
```

```
End Module
```

Through these two executables, other program can automatically update
SolidWorks model parameters and export SolidWorks CAD model to SAT file. It can
then be imported into FEA software.

Appendix B Instruction of the Structural Optimum Design Program

B.1 The description of Structural Optimum Design Program

The console program of this integrated program is written by Visual C++ language and ANSYS software is called for structural finite element analysis. Values of objective function and constraints will be output for ANSYS and be obtained by DOS command in the console program. In the part of FEA, a macro program for process control and information transformation is written by APDL (ANSYS Parametric Design Language), a built-in language of ANSYS. Structural analysis of the finite element model is performed by this macro program. At last, the approximate method is applied for numerical optimization.

B.2 The Description of Optimum Design Problem Setting

Parameter Name	Description
NParameter	Number of parameters which are inputted into system
NResponse	Number of responses generated by system
InitPar0	Initial value of design parameter #0. Change the number for other parameters.
UpperPar5	Upper boundary of design parameter #5
LowerPar1	Lower boundary of design parameter #1
UpperResp0	Upper boundary of design response #0
LowerResp2	Lower boundary of design response #2
ObjRespID	Choice a response as objective
DesignVariableIdOfPar1	Link parameter #1 to which design variable. (this interface will be changed in the future)
FiniteDifferenceStep	A FDM step of computing gradient value

B.3 The Optimum Design Problem Solver Setting

Parameter Name	Description
ErrorForDVConverge	An allowable error to determine the convergence of design variables
ErrorForObjConverge	An allowable error to determine the convergence of objective

B.4 The Approximation Setting

Parameter Name	Description
InitialMoveLimit	Define initial move limit
ReducingRatioForMoveLimit	Reducing ratio will make move limit small after each optimization iteration. The maximum range is 0.99 (99%) and it makes move limit be 1% smaller than previous iteration.
SensitivityStep	A FDM step of computing sensitivity value (default=0.001)

B.5 The Optimum Integrated Environment Setting

Parameter Name	Description
ModelSource	Choice model source. For example, 3-truss problem is computed by ANSYS, and 3D beam problem requires AutoCAD or SolidWorks and ANSYS.
ANSYSEXE	ANSYS execute file path. Ex. C:\Program Files\Ansys Inc\v100\ANSYS\bin\intel\ansys100.exe
MainWork	ANSYS main macro file.
PreWork / PostWork	Extra macro file executed before / after main macro file
UseCADModel	Select CAD model for ANSYS 0=Not require, 1=AutoCAD, 2=Inventor, 3=SolidWorks Please ensure the output file is named "model.sat"
PartForPar0	Part name of design parameter #0
NameOfPar3	Name of parameter #3 in SolidWorks part file
SWFileForOutputSAT	Name of the SolidWorks part or assembly which will be output as "model.sat"

B.6 The Macro program for structural analysis of AOI machine

```
/prep7                    ! enter the preprocessor
~satin,model              ! import the ACIS SAT file of solid model
ET,1,SOLID95              ! element type is SOLID95
AL6061=1                  ! AL6061 for first material
MP,EX,AL6061,68900        ! Young's modulus for AL6061 (first material)
MP,PRXY,AL6061,0.33       ! Poisson's ratio for AL6061 (first material)
```

```
MP,DENS,AL6061,2.7e-9    ! density for AL6061 (first material)
VGLUE,all                ! generate new volumes by gluing volumes
!==========cmsel======================================
!-----base----------      ! select the base volume as base component
allsel,all               ! select all
*GET,bottom,KP,,MNLOC,Z          ! get the minimum value of z direction in
                                   whole model
asel,s,loc,z,bottom      ! select the areas at z=min
vsla,s,0                 ! select the volume include the selected areas
cm,Base,VOLU             ! set the selected volume as a component named "BASE"


!-----4 columns & Y----------
aslv,s                   ! select all areas include the selected volume (BASE)
vsla,s,0                 ! select all volumes include selected areas (BASE and
                           volumes near BASE, like four columns)
aslv,s                   ! select all areas include the selected volume (BASE and
                           four columns)
vsla,s,0                 ! select all volumes include selected areas (BASE, four
                           columns and Y-axis beam)
vsel,u,VOLU,,Base        ! unselect BASE volume
cm,ColumnY,VOLU          ! set the selected volume as a component named
                           "ColumnY"
……                       ! repeat until all volumes are set to components


allsel,all               ! select all
MSHAPE,1,3D              ! mesh shape is set as 3D type
MSHKEY,0                 ! free meshing
ESIZE,20,                ! specify the element size
MAT,STEEL               ! specify the material name
VMESH,ColumnY           ! generate elements within ColumnY volume
……                       ! repeat until all elements are generated


/SOL                     ! enter the solution processor
*GET,bottom,NODE,,MNLOC,z        ! get the minimum value of z direction in
                                   all nodes
nsel,s,loc,z,bottom      ! select the nodes at z=min
cm,Zfix,node             ! set the selected nodes as a component named "Zfix"
D,Zfix,all,0             ! all selected nodes are fixed
```

```
allsel,all                  ! select all

ACEL,0,0,9810,              ! specify the gravity acceleration (loads)

SOLVE                       ! start a solution
/prep7                      ! enter the preprocessor
VSEL,s,VOLU,,XBeam          ! select volume named "XBeam"
VSUM                        ! compute the sum of selected volume
*GET,volume,VOLU,0,VOLU            ! get the value of VSUM
RESPONSE(1)=volume/1000000         ! define the value/1000000 as
                                   RESPONSE(1)
n_center=node(575,361,622.7)       ! select the node nearest a location
*GET,U_lens,NODE,n_center,u,sum    ! get the value of the displacement at the
                                   selected node
RESPONSE(2)=U_lens*1000            ! define the value*1000 as RESPONSE(2)
FINISH                             ! exit the postprocessor
```

B.7 The Example of Optimum Design Problem Setting

As the section 4-3:

```
[model setting]
NParameter=4                ! four design parameters
NResponse=2                 ! two responses generated by system

[solver setting]
InitialMoveLimit=2          ! initial move limit
ReducingRatioForMoveLimit=0.618     ! reduced ratio
SensitivityStep=0.005       ! a step of computing sensitivity value

InitPar0=6                  ! initial value of parameter #0

LowerPar0=5                 ! lower boundary of parameter #0
UpperPar0=30                ! upper boundary of parameter #0
UpperResp1=45.645           ! upper boundary of response #1

ObjRespID=1                 ! response #1 as the objective
```

[FEA setting]
UseCADModel=3   ! 3 is for SolidWorks

ANSYSEXE=C:\Program Files\Ansys Inc\v100\ANSYS\bin\intel\ansys100.exe
                                     ! ANSYS execute file path
MainWork=AOI.MAC   ! ANSYS main macro file

[Inventor/SolidWorks setting]
PartForPar0=AOI.SLDPRT   ! SolidWorks part name for parameter #0
NameOfPar0=d1@sketch97   ! parameter name in SolidWorks for
                                          parameter #0
SWFileForOutputSAT=AOI.SLDPRT   ! part or assembly name for outputting SAT
                                          file

VITA(作者簡歷)

Name(姓名): Chia-Hung Ma (馬嘉宏)

Date of birth(生日): 1982/07/29 (民國 71 年 7 月 29 日)

Place of birth(出生地): Taipei,Taiwan (臺灣,台北市)

Phone(電話): 02-2763-6906

Email: r95522638@ntu.edu.tw

Academic background(學經歷):

民國 77 ~ 80 年	台北縣中和市復興國小
民國 80 ~ 83 年	台北市立民權國小
民國 83 ~ 86 年	台北市立介壽國中
民國 86 ~ 89 年	台北市立西松高中
民國 89 ~ 93 年	國立臺灣大學機械工程學系
民國 93 ~ 94 年	台灣松下電器股份有限公司
民國 95 ~ 99 年	國立臺灣大學機械工程學系研究所碩士班設計組